AGU PUBLICATIONS

JGR

Journal of Geophysical Research: Earth Surface

RESEARCH ARTICLE
10.1002/2017JF004337

Key Points:
- About 40% of sediment input is trapped in the tidal Hudson, and sediment transport time scales through the estuary are years to decades
- Sediment transport in the tidal river scales linearly with the river discharge times a lag factor that increases with settling velocity
- Trapping in the tidal river corresponds with a simple advection-reaction model for settling on depositional shoals

Correspondence to:
D. K. Ralston,
dralston@whoi.edu

Citation:
Ralston, D. K., & Geyer, W. R. (2017). Sediment transport time scales and trapping efficiency in a tidal river. *Journal of Geophysical Research: Earth Surface*, *122*, 2042–2063. https://doi.org/10.1002/2017JF004337

Received 1 MAY 2017
Accepted 29 SEP 2017
Accepted article online 6 OCT 2017
Published online 2 NOV 2017

©2017. American Geophysical Union. All Rights Reserved.

Sediment Transport Time Scales and Trapping Efficiency in a Tidal River

David K. Ralston[1] **and W. Rockwell Geyer**[1]

[1]Applied Ocean Physics and Engineering Department, Woods Hole Oceanographic Institution, Woods Hole, MA, USA

Abstract Observations and a numerical model are used to characterize sediment transport in the tidal Hudson River. A sediment budget over 11 years including major discharge events indicates the tidal fresh region traps about 40% of the sediment input from the watershed. Sediment input scales with the river discharge cubed, while seaward transport in the tidal river scales linearly, so the tidal river accumulates sediment during the highest discharge events. Sediment pulses associated with discharge events dissipate moving seaward and lag the advection speed of the river by a factor of 1.5 to 3. Idealized model simulations with a range of discharge and settling velocity were used to evaluate the trapping efficiency, transport rate, and mean age of sediment input from the watershed. The seaward transport of suspended sediment scales linearly with discharge but lags the river velocity by a factor that is linear with settling velocity. The lag factor is 30–40 times the settling velocity (mm s^{-1}), so transport speeds vary by orders of magnitude from clay (0.01 mm s^{-1}) to coarse silt (1 mm s^{-1}). Deposition along the tidal river depends strongly on settling velocity, and a simple advection-reaction equation represents the loss due to settling on depositional shoals. The long-term discharge record is used to represent statistically the distribution of transport times, and time scales for settling velocities of 0.1 mm s^{-1} and 1 mm s^{-1} range from several months to several years for transport through the tidal river and several years to several decades through the estuary.

1. Introduction

Rivers provide the primary conduit for sediment delivery from continents to the coastal ocean, yet the total sediment transport that enters the coastal ocean remains difficult to constrain. Only a small fraction of global rivers have observational data on sediment delivery to the coastal zone, and in many cases those records are of only limited duration (Syvitski, 2003). In rivers that are monitored, the discharge gauges are typically located above the limit of tidal influence, and thus, sediment may be intercepted by floodplains, the tidal river, estuary, delta, and tidal flats before reaching the ocean. Many rivers have tidal fresh regions that can extend hundreds of kilometers from the coast and are thought to be significant sinks for sediment (Milliman & Farnsworth, 2013). Estimates from Amazon (Dunne et al., 1998; Nittrouer et al., 1995), Mekong (Nowacki et al., 2015), Changjiang (Milliman et al., 1985), and Ganges-Brahmaputra (Goodbred & Kuehl, 1998) indicate that one third or more the sediment delivery is trapped landward of the coast. Deltas at river mouths also represent major sinks for sediment. For example, an estimated 80% of the sediment delivered to the coastal zone by the Yellow River is deposited within its delta (Meade, 1996). Quantifying sediment trapping between the seawardmost river gauging station and the coast remains a major unknown in our ability to quantify sediment delivery to the ocean.

Sediment delivery from rivers is extremely episodic due to discharge variability, so long periods of monitoring are required to capture infrequent events to characterize the sediment load (Gray & Simões, 2008). Sediment discharge (Q_s) is often related to volumetric discharge (Q_r) by a power law relationship of the form $Q_s = a\,Q_r^{\,b}$ (Glysson, 1987; Nash, 1994). For high discharge conditions, the exponent (b) is typically 2–3, as sediment concentration increases nonlinearly with river flow due to introduction of additional sources of sediment such as bank failure. Because of the nonlinear response, a single discharge event can deliver more sediment in a few days than several years of more moderate discharge. For example in Chesapeake Bay, two discharge events were estimated to have supplied half of the total sediment over a 70 year period (Schubel & Hirschberg, 1978). Another study of Chesapeake Bay found that that the fate of sediment delivered during discharge events depended in part on the settling velocity of the particles, as finer particles during the winter bypassed the estuarine turbidity maximum (ETM) while coarser sediment during a smaller event in the fall were trapped in the ETM (Sanford et al., 2001).

While many studies have documented sediment transport and trapping in estuaries, relatively few have investigated the transport and fate of sediment in the tidal fresh river. The tidal river is the region landward of the salinity intrusion that is influenced by tides and other water level fluctuations from the coastal ocean. The landward limit of the tidal river can be a physical barrier such as a natural fall line or constructed dam, or the tidal influence can decay over a distance inland that varies depending on river discharge (Hoitink & Jay, 2016). Several studies have found significant sediment trapping in tidal rivers, either by differencing upstream and downstream transports or by measuring accretion rates. In the Amazon, an estimated 20–30% of the approximately 10^9 t yr^{-1} sediment delivery is trapped in the tidal river landward of the coast (Meade, 1996; Nittrouer et al., 1995). A reach of the tidal Amazon where two tributaries enter was found to trap 20 Mt yr^{-1} of sediment from the main stem, in addition to inputs from the tributaries (Fricke et al., 2017). In the Delaware estuary during spring freshet conditions, seaward sediment transport the upper estuary exceeded watershed inputs by more than a factor of 2, indicating that remobilization of bed sediment in the tidal river provided a major internal source (Cook et al., 2007). Similar results of seaward transport exceeding watershed input in the tidal fresh Delaware were also found over an 8 month period of moderate to low discharge (Sommerfield & Wong, 2011). Sediment budget calculations for a tributary of San Francisco Bay found that nearly 50% of the sediment input was trapped in the tidal fresh reach and that the trapping efficiency varied on the event scale from greater than 90% trapping to 30% more export than the input (Downing-Kunz & Schoellhamer, 2015). In two tributaries of Chesapeake Bay accretion rates were found to be greatest in the upper tidal fresh river and in oligohaline wetlands near the ETM, with lower accretion rates in the middle of the tidal river due to limited supply (Ensign et al., 2014).

Quantifying the delivery of sediment to the coastal ocean requires accounting for intermittent discharge events and sediment trapping in the tidal fresh region, and the Hudson River, which is the focus of this study, provides an example. In 2011, Tropical Storms Irene and Lee produced two major discharge events within a 2 week period (Ralston et al., 2013). Sediment input from the storms was 2.7 Mt based on measurements from gauges covering most of the watershed, 4–5 times the long-term annual average input. Observations in the tidal river near the limit of salinity intrusion measured seaward transport of only about 1.0 Mt, indicating significant sediment trapping in the tidal fresh region. Other studies during spring freshet conditions also found discrepancies between the sediment input and the transport in the tidal river or estuary that were indicative of extensive trapping (Wall et al., 2008; Woodruff et al., 2001). These observations lead to some basic questions about the efficiency of sediment transport in the tidal river, including sediment trapping rates and transport time scales. Sediment transport in the tidal river has important implications for the delivery of sediment to the coastal ocean, for transformations of sediment and organic particles between the watershed and the ocean, and for the recovery time scales for particle-associated contaminants. Here we use observations and a sediment transport model to evaluate sediment transport time scales and trapping efficiency in the tidal Hudson River.

2. Study Region: The Tidal Hudson River

The Hudson River discharges into New York Harbor near the Battery at the southern tip of Manhattan, and tidal influence extends landward 240 km to the Federal Dam in Troy, NY (Figure 1). Mean tidal range is 1.4 m at the Battery, decreases to 1.1 m in the middle of the tidal river, and increases to 1.5 m near the head of tide. The salinity intrusion typically varies between 40 km from the Battery (near Piermont, NY) during high discharge conditions and 120 km (near Poughkeepsie, NY) during extreme low discharge periods (Abood, 1974; Bowen & Geyer, 2003; Ralston et al., 2008). For consistency, we define the tidal fresh Hudson as the region landward of Poughkeepsie, recognizing that during moderate and high discharge periods the fresh region extends farther seaward. Hoitink and Jay (2016) define the extent of the tidal river based on water level fluctuations, with the seaward limit where the lowest water levels occur during neap rather than spring tides. Under low to moderate discharge conditions this definition does not apply to the Hudson, as lowest water levels occur during spring tides throughout the tidal reach. Instead, the Hudson generally corresponds with their "tidal freshwater zone," the reach between the salinity intrusion and the landward tidal limit. During high discharge conditions the upper ~40 km of the Hudson does have lower water levels during neap tides.

Channel depth in the Hudson decreases with distance along the river (Figure 1), from ~17 m in the saline estuary and lower fresh tidal river (with deeper regions to 40 m) to ~10 m near the tidal limit, with the

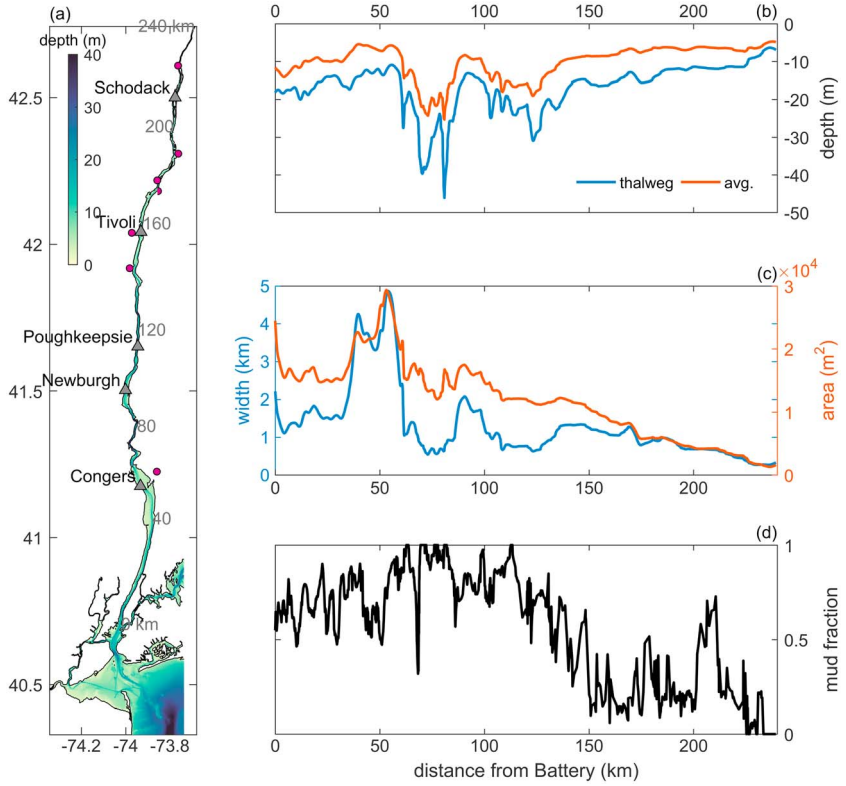

Figure 1. Hudson River bathymetry. (a) Model domain showing water depth. Observation locations are marked with triangles, and locations of tributaries discharging to the tidal Hudson are marked with circles. Distance along the river from the Battery is noted in kilometer. (b) Depth of the thalweg and cross-section average along the river. (c) Width and cross-sectional area along the river. (d) Fraction of the bed that is mud, based on the finest sediment size class in the model.

upper river depth set by dredging to an authorized depth of 32 feet (9.7 m). Cross-sectional area also decreases with distance landward, from an average width of ~1.5 km near the mouth to ~0.3 km near the head of tide. Notable wider regions include the Tappan Zee and Haverstraw Bay (35–60 km) and Newburgh Bay (85–95 km).

The Mohawk and Upper Hudson Rivers converge a few kilometers above the head of tide and provide the primary sources of freshwater and sediment to the tidal Hudson. The combined mean annual discharge from the Mohawk and Upper Hudson is about 400 $m^3\ s^{-1}$. The Mohawk represents about 30% of the total watershed area above Poughkeepsie and the Upper Hudson about 40%. Seasonally, discharge at the head of tide ranges between ~2,000 $m^3\ s^{-1}$ during the spring freshet and ~100 $m^3\ s^{-1}$ during late summer, and large events can be greater than 4,000 $m^3\ s^{-1}$. A spring freshet of 2,000 $m^3\ s^{-1}$ corresponds with a mean velocity of 0.5–1.2 m s^{-1} in the upper tidal river (>200 km), decreasing to about 0.2 m s^{-1} in the wider and deeper lower tidal river. For low discharge conditions the mean velocities associated with the freshwater outflow are 0.03–0.05 m s^{-1} in the upper tidal river and less the 0.01 m s^{-1} in the lower. Tidal velocities are significantly greater than mean velocities during low and moderate discharge conditions in most of the tidal river, typically around 0.6–0.8 m s^{-1}, but during high discharge the tide can be damped by the river flow and become unidirectionally seaward in the upper tidal river (Godin, 1999).

Sediment discharge from the Mohawk averages 0.3–0.5 Mt yr^{-1} and from the Upper Hudson 0.1–0.2 Mt yr^{-1} based on records from U.S. Geological Survey (USGS) monitoring stations at Cohoes (#01357500) and Waterford (#01335770). Sediment discharge measurements are of suspended sediment and do not include bed load, but studies of other large rivers have found that bed load represents 10% or less of the total sediment discharge (Meade, 1996). Previously reported estimates of sediment discharge to the Hudson range from 0.4 to 1.0 Mt yr^{-1}, the wide range of estimates due in part to interannual variability in the river forcing (Bokuniewicz & Ellsworth, 1986; Panuzio, 1965; Wall et al., 2008). Average

sediment yield for the Mohawk watershed (30–50 t km^{-2} yr^{-1}) is more than twice that of the Upper Hudson (10–152 t km^{-2} yr^{-1}) due to differences in geology, with clastic and glacial sediment in the Mohawk and more crystalline bedrock of the Adirondacks in the Upper Hudson. The sediment yields can be compared with an empirical model developed from a global rivers database that incorporates basin area, relief, and mean temperature (Syvitski et al., 2003). That model predicts sediment yields of about 100 t km^{-2} yr^{-1} for the Mohawk and 160 t km^{-2} yr^{-1} for the larger and steeper Upper Hudson. The factor of 2–3 overprediction for the Mohawk is typical of the model uncertainty and is consistent with the tendency of the model to overpredict sediment loads for small to moderate watersheds (Syvitski et al., 2003). The discrepancy is greater for the Upper Hudson, perhaps due to the geologic substrate and predominantly forested land use.

In addition to the Mohawk and Upper Hudson, many smaller tributaries discharge directly into the tidal Hudson (Figure 1). Collectively, these Lower Hudson watersheds represent about 30% of the total area above Poughkeepsie. The watershed downstream of Poughkeepsie is small, representing just 5% of the total watershed above the Battery. Based on observations at Poughkeepsie, the additional volume input from the Lower Hudson tributaries increases discharge by 30–40% (Wall et al., 2008). Sediment transport measurements have calculated the annual sediment discharge at Poughkeepsie between 0.7 and 1.0 Mt (Bokuniewicz & Ellsworth, 1986; Panuzio, 1965; Wall et al., 2008). Sediment input is naturally highly episodic with river discharge. For example, during a 4 year period an estimated 36% of the total sediment input occurred during just three events (Wall et al., 2008).

Suspended sediment concentrations (SSC) in the tidal river increase during high discharge. For example, tidally averaged concentrations at Poughkeepsie during the winter were 40–60 mg L^{-1} compared with 10–20 mg L^{-1} during the lower discharge summer (Wall et al., 2008). SSC also varies within a tidal cycle due to resuspension and settling. During the winter, tidal variability of 20–40 mg L^{-1} was observed at Poughkeepsie with a greater range of SSC during spring tides, compared with 10–20 mg L^{-1} tidal variability during summer. The observations suggest that a washload of fine sediment that settles too slowly to be significantly removed from the water column during slack tide represents about half of the SSC during high discharge and less than a quarter during low discharge. Water samples from this location show that the suspended sediment is dominated by fines, with 90–95% of particles <63 μm diameter, though the fine fraction decreased to 80% during a high discharge event (Wall et al., 2008). Particle settling velocities for fine sediment range from 3 mm s^{-1} for coarse silt to 0.01 mm s^{-1} or less for clay. At the upper end of this range sediment can settle at slack tide (assuming a water depth of 18 m and slack duration of 1.5 h, based on unpublished data from G. Wall), while at the lower end sediment remains in the water column as washload.

The bed sediment composition in the Hudson generally is coarser in the landward reaches (Nitsche et al., 2007). In the saline estuary and tidal fresh to near Poughkeepsie, the bed is predominantly mud or a mix of sand and mud, with the channel coarser and more erosional and the shoals finer and more depositional. The typical grain size of the bed increases landward of Poughkeepsie, with a greater sand fraction but also shallow depositional regions with finer sediment. Through much of the tidal river and estuary, both fine-grained, depositional areas and coarser-grained, erosional channel regions can be found in the same segment of river. Landward of about 200 km the river is predominantly erosional and dominated by sand and gravel size classes.

Most of the tidal Hudson is thought to be at equilibrium depth and accreting at a long-term rate approximately equal to sea level rise (0.3 cm yr^{-1}) based on ^{14}C chronology (Klingbeil & Sommerfield, 2005; McHugh et al., 2004). Shorter time scale measurements using ^{137}Cs and ^{210}Pb typically show higher accumulation rates, for example, in the tidal river rates of 0.6–2.9 cm yr^{-1} at 160 km (Benoit et al., 1999) and 1.5–1.8 cm yr^{-1} at 143 km (Chillrud et al., 2004). Even greater short-term accretion rates have been reported in the saline estuary with 10–40 cm yr^{-1} at seasonal time scales based on ^{7}Be (Feng et al., 1998; Traykovski et al., 2004; Woodruff et al., 2001). These shorter time scale deposition rates are highly variable in space and time and can be an order of magnitude greater than the long-term average due to redistribution of deposited sediment during erosional events and compaction of bed sediment (Sommerfield, 2006). Based on ^{14}C, the saline estuary is also accumulating sediment at a rate similar to sea level rise (1.6–3.5 mm yr^{-1}) over 400–3,000 year time scales (Klingbeil & Sommerfield, 2005).

3. Methods

3.1. Observations

Observational data were collected from several sources, including instruments deployed for this study and from long-term monitoring stations maintained by the U.S. Geological Survey (USGS) and the Hudson River Environmental Conditions Observing System (HRECOS). Study periods spanned a range of river discharge conditions, included the high discharge events associated with Tropical Storms Irene and Lee in summer 2011 (maximum discharge at the head of tide, $Q_{r,max}$ = 4,400 m^3 s^{-1}), a moderate spring freshet in 2014 ($Q_{r,max}$ = 2,500 m^3 s^{-1}), and a smaller than average freshet in 2015 ($Q_{r,max}$ = 1,300 m^3 s^{-1}).

Time series of river and sediment discharge were obtained from the USGS for the Mohawk River at Cohoes (1917 to present) and the Upper Hudson River at Waterford (1887 to present). Daily sediment discharge measurements are available for the Mohawk for 1954–1959, 1976–1979, and 2004–2015 and for the Upper Hudson for 1976–2014. River discharge and in some cases sediment discharge were also obtained for tributaries of the Lower Hudson River, including Normans Kill (#01359528), Kinderhook Creek (#01361000), Catskill Creek (#01362090), and Roeliff Jansen Kill (#01362182), Esopus Creek (#01364500), Rondout Creek (#01367500), and Croton River (#01375000). Volume and suspended sediment transports were obtained in the tidal river at Poughkeepsie (#01372058) for 2002–2014. Details on the Poughkeepsie observations and analysis from 2002 to 2006 are in Wall et al. (2008). In addition to the USGS stations, turbidity time series (15 min sampling interval) were obtained from HRECOS stations on the tidal river including Schodack Island (214 km), Tivoli Bays South (160 km), and Norrie Point (134 km).

Observations from 2011 after Tropical Storms Irene and Lee came from USGS and HRECOS stations and have been reported previously (Ralston et al., 2013). In 2014 and 2015 observations were collected at three additional locations: Tivoli (160 km), Newburgh (90 km), and Congers (55 km) (Figure 1). Each location had optical backscatter sensors (OBS) to measure turbidity at the surface and bottom (1 min sampling interval). OBS data from these deployments and from the HRECOS stations were downsampled to hourly intervals using a median filter to reduce noise. In 2014, extensive ice coverage delayed the start of observations until 31 March, shortly before with the first discharge event of the spring. Instruments were recovered 10 June 2014 when discharge at the head of tide had decreased to less than 200 m^3 s^1. The second deployment was from 8 December 2014 to 15 May 2015, and discharge was generally lower than average throughout the spring 2015.

Surface and bottom water samples were collected during each deployment and processed for total suspended sediment to calibrate the OBSs. The calibration between turbidity (NTU) and SSC (mg L^{-1}) from samples during the 2014 spring freshet (31 March to 1 April) resulted in a regression slope of 0.6 (SSC $\approx 0.6 \times$ NTU). Previous observations in the saline estuary using the same methods have typically found slopes of around 1 (Ralston et al., 2012), and this lower slope suggests a shift in sediment size toward smaller particles during high flow conditions (Downing, 2006). For samples taken during the lower discharge conditions of 2015 (13–14 May), the slope from the calibration was 1.1. Suspended sediment samples were also processed for loss on ignition (LOI), a measure of organic content. The LOI was less than 1% in the high discharge samples of 2014, while LOI was 8–12% for the lower discharge samples of 2015. The shift in both the turbidity to SSC calibration and LOI are consistent with a greater prevalence of silt and clay particles from the watershed during the first major discharge event of the season in 2014, in contrast to 2015 when the turbidity signal was lower (shown below) and dominated by resuspended bed material with larger particles and greater organic content.

3.2. Circulation and Sediment Transport Model

Simulations of the tidal Hudson River and estuary using realistic and idealized forcing were run using the Regional Ocean Modeling System (ROMS) with the Community Sediment Transport Modeling System (Haidvogel et al., 2008; Shchepetkin & McWilliams, 2005; Warner et al., 2008). The Hudson model has been developed and evaluated against observations over a series of previous studies (Ralston et al., 2012, 2013; Warner et al., 2005, 2010). The curvilinear model grid included the landward limit of the tidal river to open boundaries in New York Bight and Western Long Island Sound (Figure 1). The grid was 1,135 cells by 532 cells, with grid resolution of 100 to 500 m along channel that decreased in resolution toward the tidal limit and 20–60 m grid resolution laterally. The vertical discretization had 16 evenly distributed sigma layers.

For the realistic simulations, freshwater and suspended sediment were input from the Mohawk and Upper Hudson Rivers and from the seven tributaries discharging directly to the Lower Hudson (listed above). Discharges were based on USGS observations, and suspended sediment concentrations were based on USGS observations (when available) or on rating curves developed from observations (Woodruff, 1999). Water level at the open boundary was forced with tidal constituents from an ADCIRC database (Mukai et al., 2002) plus a lower frequency, nontidal component based on a low-pass filter of water level observations at Sandy Hook, NJ (NOAA #8531680) and Kings Point, NY (NOAA #8516945). Observational data for discharge and water level had 15 min temporal resolution, except for four of the smaller rivers that only had daily data. Model fields were saved at hourly intervals for analysis.

Sediment in the realistic cases had five independent sediment classes: three on the bed at the start of the simulation and two with river inputs. On the bed, the size classes were representative of medium sand (settling velocity, $w_s = 40$ mm s^{-1}), fine sand ($w_s = 5$ mm s^{-1}), and medium silt ($w_s = 0.6$ mm s^{-1}). The river sediment classes were fine silt (0.2 mm s^{-1}) and very fine silt or clay (0.01 mm s^{-1}). The settling velocities of the river sediment classes were based on previous comparisons with observations in the tidal river (Ralston et al., 2013). Maps of bed sediment composition based on side scan surveys and bottom samples (Nitsche et al., 2007) were used to initialize the fraction of each size class on the bed, and this was run for several months with typical forcing conditions to create an initial condition for subsequent simulations. The bed had a single layer with a uniform initial thickness of 0.2 m for most cases, as discussed below. In model simulations the maximum erosion was typically a few centimeters or less, so with this initial condition the bed sediment supply was not depleted. Exchange between the bed and water column was calculated in the ROMS based on the settling velocity and excess shear stress as described in Warner et al. (2008) using erosion rate parameters determined previously for the Hudson based on comparison with observations (Ralston et al., 2012).

To diagnose how river discharge and settling velocity affect transport rates, we also ran several idealized simulations. For idealized cases, river and sediment discharge were applied only at the head of tide and harmonic tides with only M_2, S_2, and N_2 components were applied at the open boundaries. The idealized cases included using relatively slow settling velocities ($w_s = 0.01$ and 0.2 mm s^{-1}) from the realistic simulations over a range of constant discharge cases (Q_r = 150, 300, 600, 2,000, and 5,000 m^3 s^{-1}) as well as testing a wider range of settling velocities (w_s = 0.03, 0.1, 0.3, 1, and 3 mm s^{-1}) for a constant discharge of 5,000 m^3 s^{-1}. As will be shown, the dependence on settling velocity was largely independent of discharge. The system reaches equilibrium for suspended sediment transport more slowly for low discharge cases than for high, and similarly fast settling sediment takes longer to reach equilibrium than the washload. To make the model computationally tractable and evaluate the range of settling velocities, we focus on results from the high discharge case. Lower discharge cases would show similar dependence on settling velocity but would require proportionally longer run times.

3.3. Sediment Age

To characterize the time scales of sediment transport, we modified the age calculation in ROMS that was previously used to track the chronology of water parcels (Zhang et al., 2009) to apply to sediment. The mass-weighted, arithmetic age of a tracer or sediment is calculated following the constituent-oriented age and residence-time theory (CART) (Deleersnijder et al, 2001; Delhez et al., 1999). The approach introduces an age concentration tracer that corresponds with each constituent being evaluated. Transport of the age concentration tracer in the model is treated exactly as the corresponding tracer, but the age grows in time with each model time step. The mean age of a tracer is a three-dimensional, time-dependent quantity equal to the age concentration divided by the tracer concentration.

The application of CART to calculate sediment age was previously developed for a study of sediment transport off the Belgian coast (Mercier & Delhez, 2007). The definition of the start time (or zero age) for a constituent is key to the age calculation, and the specification depends on the goals of the study. Mercier and Delhez (2007) presented two complementary approaches to sediment age. Their "resuspension age" was set to zero when sediment was resuspended and increased while sediment was in the water column, so age represented the time since the sediment was last on the bed. Their "transport age" was reset to zero when sediment left a source region, and sediment continued to age both in the water column and on the bed. We apply this transport age in the Hudson simulations and define the source region for zero age to be when sediment enters from the watershed. A similar application of the transport age approach was

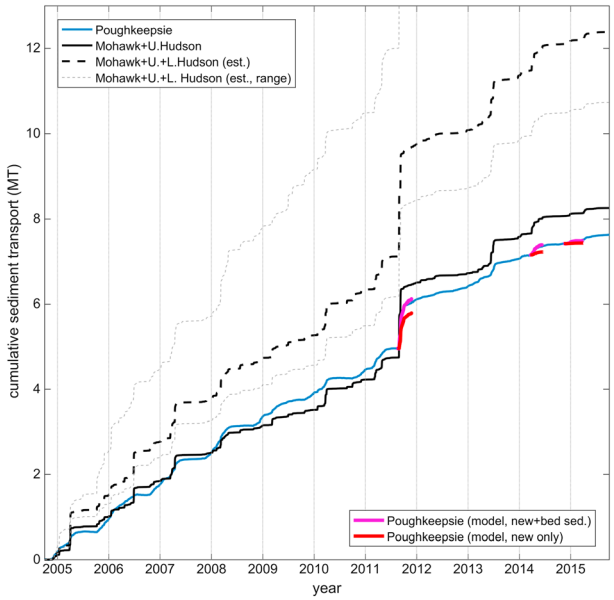

Figure 2. Cumulative sediment transport in the tidal Hudson. Observed transport at Poughkeepsie is based on measured velocity and suspended sediment (USGS), or when that is not available, on velocity at Poughkeepsie and suspended sediment from turbidity at Norrie Point (HRECOS). Measured sediment inputs for the Mohawk and Upper Hudson are shown, along with a range of estimates for the additional inputs from Lower Hudson tributaries, as noted in the text. Cumulative sediment transport at Poughkeepsie for each of the model periods (2011, 2014, and 2015) is shown for both new sediment from the watershed and new sediment plus remobilized bed sediment.

used to track watershed sediment input to the York River estuary (Gong & Shen, 2010). Transport age was also used to examine transport of contaminants adsorbed to sediment in the Scheldt estuary, where the approach was extended to keep track separately of the time sediment spends in the water column and time on the bed (Delhez & Wolk, 2013).

As it moves through the system, sediment ages with a spatial distribution that depends on the hydrodynamic conditions and sediment characteristics. Sediment ages with each model time step both in the water column and on the bed after deposition. The age concentration variable behaves exactly the same as the sediment concentration, so that sediment settles with its age and is eroded with the average age of the sediment on the bed at each location (Gong & Shen, 2010; Mercier & Delhez, 2007). Transport of age concentration in the water column includes the vertical settling velocity for each sediment class in addition to advection by the three-dimensional velocity field. The settling velocity and erosion rates for age concentration are the same as those for the corresponding sediment class.

4. Results

4.1. Sediment Transport and Mass Accumulation

The major discharge events associated with Tropical Storms Irene and Lee in late summer 2011 delivered about 2.7 Mt of new sediment to the tidal Hudson. Due to the rainfall distribution, disproportionate sediment loading came from the Mohawk (1.4 Mt, 30% of the total watershed area) and from several tributaries discharging directly to the tidal Hudson, in particular Catskill Creek (0.7 Mt, 3% of total watershed, at 180 km) (Ralston et al., 2013). At Poughkeepsie, the cumulative transport during the months following the storms was about 1.0 Mt, indicating that a substantial fraction of the sediment input remained in the tidal river for a period much greater than the event or spring-neap time scales. Fortunately, the Irene and Lee events occurred during a period of expanded monitoring by the USGS of sediment discharge from the watersheds of the Lower Hudson. Streamflow and suspended sediment concentrations were recorded at stations representing most of the total watershed area, allowing quantification of the sediment budget to an uncommon precision.

One of the key uncertainties in the sediment budget is the loading from tributaries discharging directly to the tidal Hudson. For Irene and Lee, the Lower Hudson tributaries added sediment loading equal to 70% of that from the Mohawk and Upper Hudson. An estimate based on the transport at Poughkeepsie over 4 years calculated that the Lower Hudson increased the sediment load by 30–40% (Wall et al., 2008). As with Irene and Lee, the largest imbalances between the input at the head of tide and the transport past Poughkeepsie were due to high discharge events. In another study, contaminant metal profiles from sediment cores along the tidal fresh Hudson were the basis for an estimate that Upper Hudson sediment was being diluted by a factor of 8 by inputs from the Mohawk and downstream tributaries (Chillrud et al., 2004). The sediment load from the Mohawk on average is 2.6 times that of the Upper Hudson, so the dilution of contaminant metals observed in the cores requires additional input from the Lower Hudson that is similar in magnitude to the combined input from the Upper Hudson and Mohawk. A watershed model accounting for differences in land use suggested that sediment yield for the Lower Hudson was greater than for the Upper Hudson (Swaney et al., 1996), consistent with input greater than the watershed area ratio.

Daily averaged sediment discharge measurements are available for the Mohawk, Upper Hudson, and tidal fresh Hudson at Poughkeepsie for most of 2004–2015 (Figure 2). For the periods when SSC data are not available at Poughkeepsie (September 2011 to January 2014 and October 2014 to October 2015), SSC data from Norrie Point are paired with the volumetric discharge at Poughkeepsie. During Irene and Lee, Norrie Point turbidity correlated well with turbidity observed at Poughkeepsie (Ralston et al., 2013). Turbidity at Norrie is converted to SSC based on a calibration from bottle samples. To estimate the total sediment load to the

tidal river including tributaries of the Lower Hudson, the observed transport from the Mohawk and Upper Hudson is multiplied by a factor of 1.5. This is based on an average of previous estimates of 1.3 (Wall et al., 2008) and 1.7 (Ralston et al., 2013) and is less than the 2.2 factor derived from cores (Chillrud et al., 2004). Over this 11 year record, the cumulative input from the Mohawk and Upper Hudson was 8.2 Mt, and with the 1.5 factor for the Lower Hudson the total input was 12.4 Mt. At Poughkeepsie, the cumulative seaward transport was 7.6 Mt, somewhat less than the input from the Mohawk and Upper Hudson and about 60% of the total estimated input from the watershed.

The trend over this 11 year period indicates that some 40% of the sediment input remains trapped in the fresh tidal river for an extended period. The spatial extent of the tidal river above Poughkeepsie is about 110 km^2 (120 km of river with average width of ~900 m), so assuming a bulk density of 500 kg m^{-3} the calculated mass accumulation distributed evenly would correspond with a depositional thickness of 8.5 cm. Sea level rise at the Battery (NOAA #8518750) averaged 3.38 mm yr^{-1} over 1975–2015, so the increase in accommodation space (3.7 cm over 11 years) could account for approximately half of the sediment trapping. The depositional area may be an overestimate given that large parts of the tidal fresh Hudson are sandy and nondepositional (Nitsche et al., 2007), but additional sediment storage is possible on flood plains or in off-river water bodies, where accumulation rates can greatly exceed sea level rise (Woodruff et al., 2013). Cores from depositional regions along the tidal fresh Hudson have been found to have accumulation rates in excess of 1 cm yr^{-1} (Benoit et al., 1999; Chillrud et al., 2004).

Previously, the cumulative sediment transport past Poughkeepsie after Irene and Lee in the model was found to be similar to observations (Ralston et al., 2013). The settling velocity associated with the sediment input was a critical parameter that was adjusted to improve the model agreement. The watershed inputs were split into sediment classes with w_s = 0.2 mm s^{-1} (17 m d^{-1}) and 0.01 mm s^{-1} (0.8 m d^{-1}), corresponding, respectively, with particle sizes of fine-to-medium silt and fine silt or clay. We show later that the mean advection speed for sediment depends inversely on settling velocity, so the timing and quantity of mass transport in the model depends on the fraction of the total sediment input assigned to the washload. For Irene and Lee, assigning 20% of the new sediment input to the washload size class agreed with the mass transport observations, so that ratio is used in the simulations in this study. The Irene and Lee model results also demonstrated that matching the timing of the transport past Poughkeepsie required including remobilization of bed sediment in the river prior to the events. The total transport in the model then depends not only on the watershed inputs but also the availability of erodible sediment in the bed.

The model was run for the observational periods in 2014 and 2015 with the configuration from the calibration to Irene and Lee in 2011, and the net transport in the model at Poughkeepsie compares well with the observations (Figure 2). Again, the total mass transport, including remobilized bed sediment, is closer to the observations than the newly input sediment alone. The year 2014 had a typical spring freshet, and the total sediment transport past Poughkeepie during the simulation period (85 days) was 0.20 Mt in the observations and 0.24 Mt in the model, while watershed input was 0.35 Mt. In 2015, the freshet discharge was smaller than average and the sediment transport was reduced, with 0.087 Mt observed past Poughkeepsie and 0.067 modeled over 135 day period, compared with 0.071 Mt of watershed input.

Both the observations and model reflect the strong dependence on discharge of the sediment loading and the transport in the tidal river. For the Mohawk the sediment discharge rating curve is $Q_s \sim Q_r^{1.35}$ for $Q_r < 500$ m^3 s^{-1} and $Q_s \sim Q_r^{2.87}$ for higher discharge (Woodruff, 1999). In the Upper Hudson the relationships are similar, with $Q_s \sim Q_r^{1.43}$ for $Q_r < 400$ m^3 s^{-1} and $Q_s \sim Q_r^{2.87}$ for greater Q_r. Because of the nearly cubic dependence, sediment loading is dominated by large, infrequent events. In contrast, the relationship between river discharge and sediment transport at Poughkeepsie in both observations and the model is less than a cubic dependence (Figure 3). Trend lines for cubic and linear dependence on discharge are shown for reference. Linear dependence corresponds with a suspended sediment concentration that is independent of river discharge, if, for example, SSC is controlled by resuspension of bed sediment by tidal currents alone and is independent of discharge.

During the peak flows of Irene and Lee, watershed input exceeded the observed transport in the tidal river by an order of magnitude, but at intermediate discharges the seaward transport at Poughkeepsie was similar to or greater than the watershed input. The interannual variability in transport at intermediate discharges depends in part on the availability of mobile sediment, which depends on the antecedent loading to the

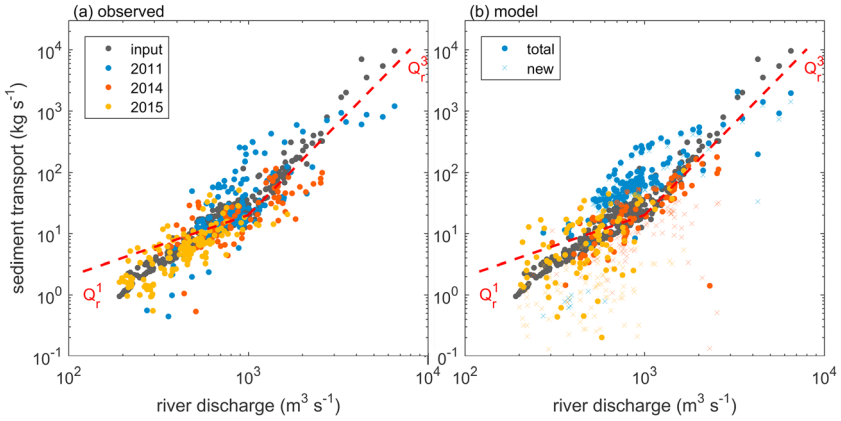

Figure 3. Sediment transport versus river discharge. (a) Daily average sediment input from rivers (black) and sediment transport at Poughkeepsie during 2011, 2014, and 2015 observation periods. (b) Sediment transport at Poughkeepsie in the model during the same periods; river inputs are the same. Large dots are the total sediment transport including remobilized bed sediment, and small crosses are newly input sediment from the rivers.

system (Woodruff et al., 2001). In 2011, the supply of mobile sediment in the tidal river was enhanced due to the inputs from the two storms, and consequently, sediment concentrations were greater at given discharge than in the subsequent years. Overall, the transport at Poughkeepsie scales roughly linearly with river discharge, with the magnitude of the linear dependence varying due to antecedent loading. Assuming that at long time-scales the system is at morphodynamic equilibrium, the mismatch in scaling between the nearly cubic sediment supply and the linear transport requires that there is a net sediment gain to the tidal river during brief high discharge events and net loss over longer periods of intermediate discharge (Ralston & Geyer, 2009). Sediment accumulation during events and loss during lower discharge is consistent with analysis of a 4 year record at Poughkeepsie (Wall et al., 2008). The dependence of transport in the tidal river on discharge in the model is similar to observations, but only when including remobilized bed sediment (Figure 3b).

4.2. Sediment Transport Time Scales

The discrepancy in discharge dependence between the loading and sediment transport in the tidal river raises questions not only of total mass transport but also of timing. Observations of turbidity at multiple locations along the tidal fresh river illustrate the advection of the sediment pulses due to discharge events (Figure 4). In 2011, Irene and Lee ($Q_{r,\max} \approx 3{,}900$ and $3{,}300\ m^3\ s^{-1}$ at the head of tide) provided distinct peaks in turbidity at Schodack (214 km), Tivoli (160 km), and Norrie Point (134 km). The seaward advection of the turbidity pulse can be compared with the fluvial advection speed based on the mean river velocity, $u_r = Q_r/A$, where A is the average cross-sectional area of the river. The turbidity pulse moved seaward more slowly by a factor of 1.5 to 2 than the mean advection time between the stations. The calculation was based on the arrival time of the peak turbidity for each discharge event, which has uncertainty that grows as the turbidity pulse spreads downstream.

In the spring of 2014, three distinct discharge events ($Q_{r,\max} \approx 3{,}200$, 3,000, and $2{,}100\ m^3\ s^{-1}$) were associated with spikes in turbidity through the tidal river, including at sensors at Newburgh (90 km) and Congers (55 km) (Figure 4b). The spring of 2015 had lower discharge, with only a single event ($Q_{r,\max} \approx 1{,}800\ m^3\ s^{-1}$) that had a distinct turbidity signal. At the more seaward observation locations the turbidity maxima from the events become more diffuse and hard to identify, and instead, the spring-neap cycle was most prominent in the temporal variability. While the mean flow U_r is responsible for the net seaward transport, tidal velocities that are typically an order of magnitude greater enhance along-river dispersion of the turbidity pulse. For the larger discharge events that could be tracked, the turbidity pulses moved seaward at rates slower than river flow. The transport time between stations was 1.5 to 3 times the transport time for water, with the factor increasing with distance downstream. Note that the turbidity signal may represent only part of the sediment input and transport. Optical backscatter measurements of turbidity are more sensitive (on a mass basis) to the

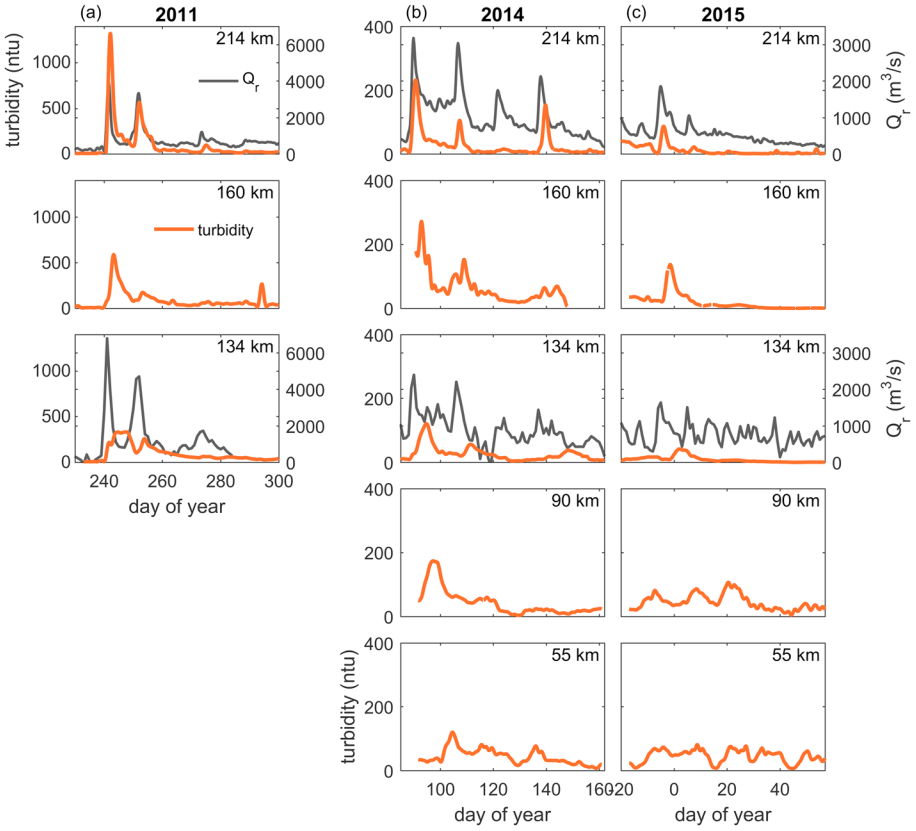

Figure 4. Observed time series of turbidity along the Hudson at Schodack (214 km), Tivoli (160 km), Norrie Point (134 km), Newburgh (90 km), and Congers (55 km) during the 2011, 2014, and 2015. Note that the turbidity axis range for Figure 4a is 3.5 times greater than for Figures 4b and 4c. River discharge at the head of tide and mean flow at Poughkeepsie are shown in black on the right axis.

finer, slower settling particles that are transported most rapidly than coarser silt and sand that move seaward more slowly, as will be shown.

The model results provide a more continuous picture in time and space of the suspended sediment transport from discharge events (Figure 5). The spring freshet of 2014 is used as an example, but similar results were found for 2011 (Ralston et al., 2013) and for 2015. Three events provided significant sediment loading, and the advective time scale based on Q_r/A for each is noted for reference. Note that this realistic simulation includes river and sediment discharge from lateral tributaries of the Lower Hudson that provide sediment prior to the arrival of the pulse from the Mohawk and Upper Hudson. The model results illustrate spatial variability that is not resolved by the observational time series, as greater suspended sediment concentrations are consistently found in particular sections of the river. The events highlight these local trapping regions, but as each sediment pulse propagates seaward and disperses it lags the speed of the river flow. The realistic results for 2014 (Figure 5) combine sediment classes with 0.01 and 0.2 mm s^{-1} based on the Irene and Lee calibration, and the sediment transport rate relative to river advection is sensitive to settling velocity, as will be examined later with idealized model cases.

The along-river distribution of new sediment at the end of the simulation, both in suspension and on the bed, highlights the regions of intensified trapping (Figure 5c). Over approximately 3 months, about 0.34 Mt of sediment was introduced, predominantly during the discharge events 10 and 15 days into the simulation. At the end of the simulation, about 85% of that new sediment remained trapped above the limit of the salinity intrusion, located at 90 km at that time. Much of the new sediment in the saline estuary was trapped in the upper ETM of Haverstraw Bay (55 km) (Nitsche et al., 2010; Ralston et al., 2012). Less than 1% of the new sediment input had moved seaward of the Battery after 3 months. As with the rate of seaward transport, we will use

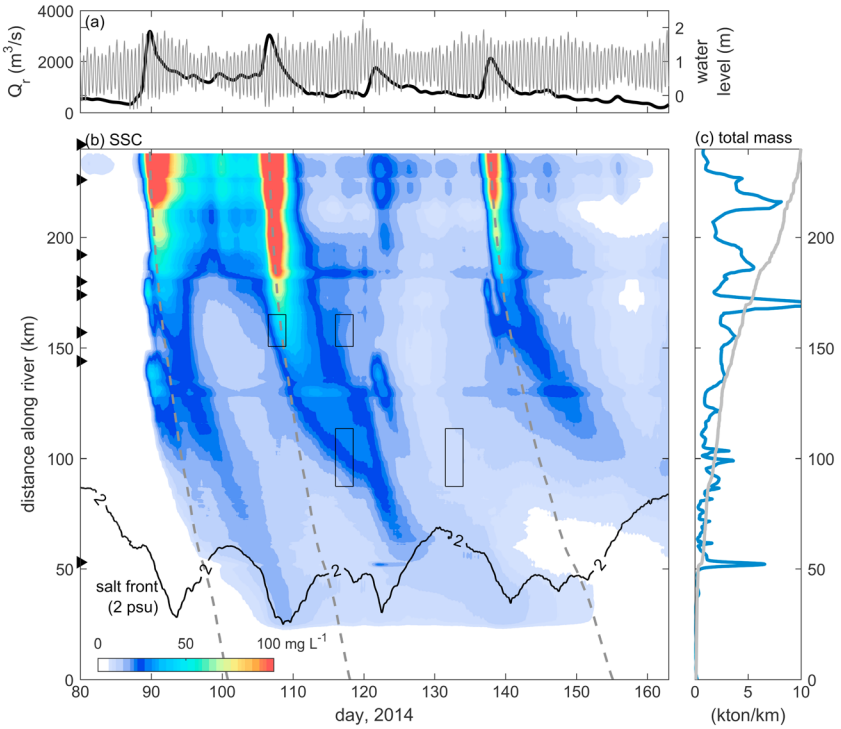

Figure 5. Modeled time series of suspended sediment from river inputs in 2014. (a) River discharge at the head of tide and water level at the Battery. (b) Cross sectionally averaged suspended sediment concentration from river inputs as a function of distance along the river and time. Locations of tributary inputs are marked with triangles on the *y* axis. The rate of advection associated with the three largest discharge events (distance = $\Sigma(Q_r/A)\Delta t$) is marked with a gray dashed line. The 2 psu isohaline of bottom salinity is marked in black. Boxes highlight the periods and locations shown in Figure 6. (c) Total sediment mass (suspended + bed) at the end of the model period. Gray line is the cumulative mass distribution from the seaward boundary to the head of tide normalized by the total mass.

idealized cases to examine how this sediment trapping in the tidal river (or inversely, the transport efficiency) depends on the settling velocity.

As the suspended sediment pulse associated with each discharge event moved seaward, the maximum concentration decreased and the sediment signal dispersed along the river. Tidal velocities continued to remobilize and move sediment after the event, and sediment was preferentially deposited in lower energy regions on the shoals and side embayments. Examples during and after the arrival of a sediment pulse demonstrate the temporal decrease in SSC in the channel correspond with an accumulation of deposited sediment on shoals and inside embayments (Figure 6). The maps also illustrate the lateral variability in suspended sediment concentration and trapping, indicating that the observational time series of turbidity may be sensitive their location in the cross section.

4.3. Transport Time Scales With Idealized Forcing

The transport in the tidal river near Poughkeepsie (120 km) for an extended period with a constant discharge of 5,000 $m^3\ s^{-1}$ illustrates the dependence on settling velocity of both the timing and the magnitude of transport (Figure 7). With the exception of the fastest settling sediment (3 mm s^{-1}), transport at Poughkeepsie reached equilibrium values that modulated with spring-neap variability. The time scale to reach equilibrium was several days to months depending on settling velocity, as will be discussed below. For the slowest settling sediment (w_s = 0.03 mm s^{-1}), the equilibrium transport was almost 90% of the input at the head of tide, and the transport relative to the input decreased as settling velocity increased, to 67%, 36%, 7%, and less than 1% for w_s = 0.1, 0.3, 1, and 3 mm s^{-1}, respectively. The transport in each sediment class was greater at more landward cross sections and less at more seaward locations, but at each position along the tidal river the transport decreased with greater settling velocity (Figure 7c).

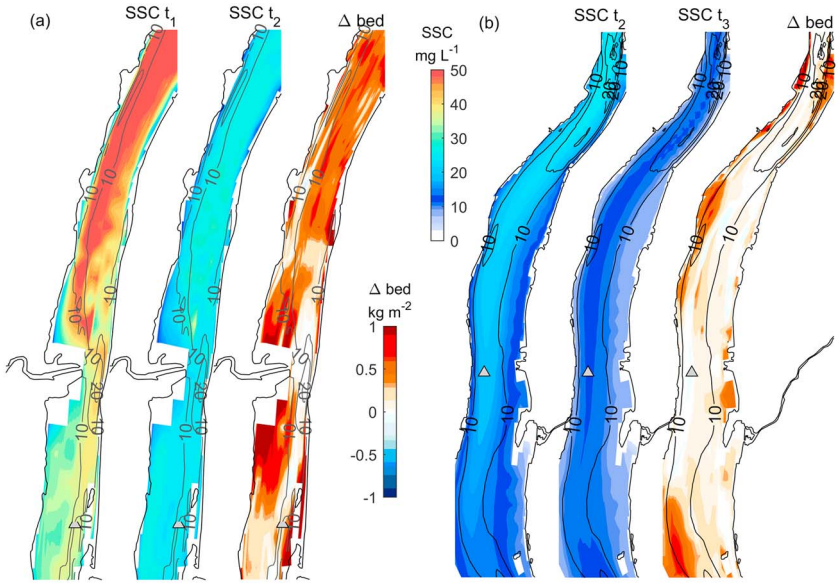

Figure 6. Maps of average suspended sediment concentration from river inputs for two time periods and the net change in sediment mass on the bed between the periods. Selected times are during a period with increased sediment concentration from a discharge event and then 10–15 days after. Two regions are shown: (a) near Tivoli and (b) near Poughkeepsie and Newburgh; locations of the observations are marked with gray triangles. The times and locations of the maps are marked in Figure 5.

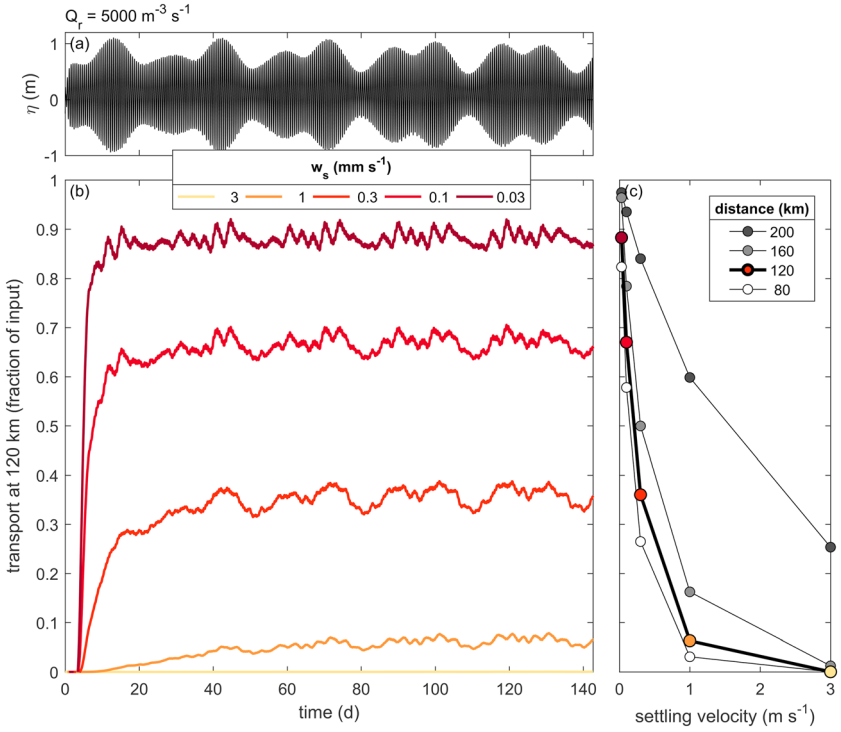

Figure 7. Sediment transport dependence on settling velocity. (a) Idealized tidal forcing for the constant discharge case of Q_r = 5,000 m^3 s^{-1}. (b) Time series of tidally filtered sediment transport at 120 km (near Poughkeepsie) for sediment classes with settling velocity spanning 0.03 to 3 mm s^{-1}. (c) Sediment transport at the end of the simulation period for different locations along the river (80, 120, 160, and 200 km) versus settling velocity. The colored dots correspond with the full time series in Figure 7a.

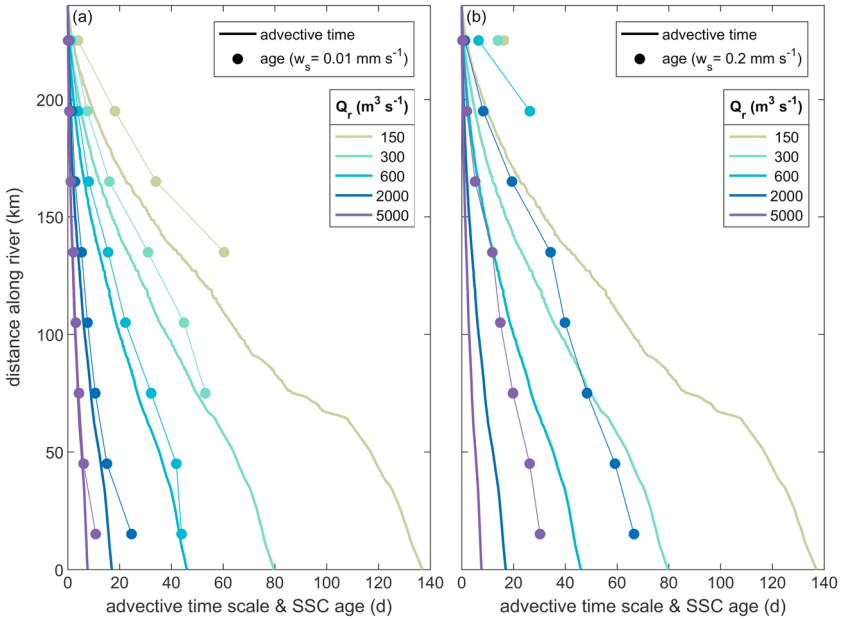

Figure 8. Advective time scales and sediment age. In both panels, solid lines are the advective time scale (distance/(Q_r/A)) versus distance along the river for different constant discharge cases (150, 300, 600, 2,000, and 5,000 m^3 s^{-1}). (a) Solid circles are the average age of suspended sediment with settling velocity = 0.01 mm s^{-1} versus distance along the river for the same constant discharge cases, where suspended sediment age has been averaged in 30 km bins along the river. (b) Same but for settling velocity = 0.2 mm s^{-1}.

The time required to reach the equilibrium seaward transport also depended on settling velocity (Figure 7b). Taking the time to reach 75% of the equilibrium transport for each class, the w_s = 0.03 mm s^{-1} sediment had a time scale of about 5.6 days, while the 0.3 mm s^{-1} sediment was 14 days. A case with Q_r = 5,000 m^3 s^{-1} but an initial bed thickness of 0.02 m (rather than 0.2 m) resulted in similar equilibrium transport for each sediment class, but the time to approach equilibrium was faster: 5.2 days for w_s = 0.03 mm s^{-1} and 6.0 days for 0.3 mm s^{-1}. The time scales to reach equilibrium for the slower settling sediment were much longer than most 5,000 m^3 s^{-1} discharge events, but the high flow case provides an efficient means of quantifying transport rates that are slow compared with the natural time scales of discharge.

The transport time scale can also be characterized based on sediment age, which increases from the time sediment is input at the head of tide. Sediment age is compared with the advective time scale, or the age that a parcel of water moving at the mean river velocity would have with distance along the river (Figure 8). For example, at 5,000 m^3 s^{-1} the advective time scale to Poughkeepsie (120 km) was just over 2 days and to the Battery (0 km) was about 7 days because the mean velocity decreases as the cross-sectional area increases toward the mouth. At 150 m^3 s^{-1} the transport time to Poughkeepsie was almost 2 months and to the Battery was 4.5 months.

Across the constant discharge cases, the age of suspended sediment paralleled the advective time scale with distance along the river (Figure 8). Sediment age was averaged in 30 km bins along the river, and results are only shown for regions with enough sediment at the end of the simulation to calculate a meaningful age. Faster settling and, therefore, slower moving sediment were found only in the upper reaches, as sufficient mass did not reach the lower river by the end of the simulations. For the more slowly settling sediment (w_s = 0.01 mm s^{-1}), sediment age lagged the advective time scale for water only slightly, but the lag was greater for the faster settling class (w_s = 0.2 mm s^{-1}) in all the discharge cases. The time lag decreased as discharge increased because sediment age depended on the advective time scale, as is examined next.

Comparison of the advective time scale with sediment age for all the discharge cases results in a linear relationship that depends on settling velocity (Figure 9). Using the range of discharge cases, the best fit slope was 1.3 for w_s = 0.01 mm s^{-1} and the slope was 5.0 for w_s = 0.2 mm s^{-1} (Figure 9a). The slope represents the factor

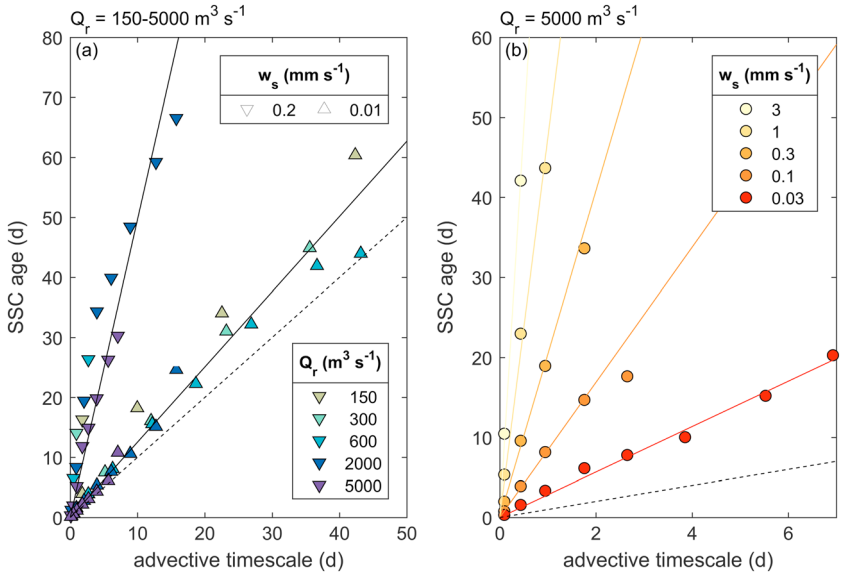

Figure 9. Advective time scale versus suspended sediment age. (a) A range of constant discharge cases (150, 300, 600, 2,000, and 5,000 $m^3\ s^{-1}$) with settling velocity = 0.01 and 0.2 mm s^{-1} (as in Figure 8). (b) Constant discharge with 5,000 $m^3\ s^{-1}$ and a range of settling velocities (0.03, 0.1, 0.3, 1, and 3 mm s^{-1}). Solid lines are best fit slopes and dashed lines are a slope of 1. Suspended sediment age has been averaged in 30 km bins along the river, and only the bins with sufficient sediment to calculate a meaningful age at the end of each simulation are shown.

by which the average age of suspended sediment lags the advective time scale, so we can write a scaling for mean age of suspended sediment (a_{ssc}) based on those factors:

$$a_{ssc} = \lambda_{ws} t_{adv} \quad (1)$$

where λ_{ws} is the slope or lag factor and t_{adv} is the advective time scale for water. The linear scaling holds across the wider range of settling velocities used in the Q_r = 5,000 $m^3\ s^{-1}$ case (Figure 9b). For w_s = 0.03 mm s^{-1}, the lag factor of 2.8 represented the sediment age over the full length of the tidal river. For the 3 mm s^{-1} sediment, the transport rate was much slower and the best fit slope was 98. Modeling studies of the York River also found that sediment transport age increased for greater settling velocity, with sediment age at the mouth of the estuary exceeding the age of water by a factor of about 1.5 for settling velocity of 0.01 mm s^{-1} and a factor of about 6 for settling velocity of 0.05 mm s^{-1} (Gong & Shen, 2010). In the York sediment age also decreased as discharge increased, as was found for the age of contaminants adsorbed to sediment in the Scheldt Estuary (Delhez & Wolk, 2013).

In the Hudson, the faster settling sediment classes were limited to the upper river due to their higher rates of deposition (Figure 7) and slower rates of transport (Figure 9b), so the slope estimates were based on a few data points and were less well constrained. The spatial heterogeneity of the bathymetry introduces variability in transport and consequently the age distribution, but the linear relationship between the advective time scale and sediment age does not vary notably with distance along the river. The suspended sediment age was not dominantly affected by interaction with the bed sediment because most of the seaward mass transport occurred in the deeper, higher stress channel, where suspended sediment may deposit briefly at slack tide but then is resuspended without much long-term accumulation. As is shown later, depositional regions at channel edges accumulate sediment that can resuspend as a source of older sediment, but the dominant suspended sediment transport occurs in the channel.

Based on the idealized model cases spanning discharge and settling velocity parameter space, we evaluated the relationship between settling velocity and the lag in sediment transport rate or specifically the suspended sediment age relative to the advective time scale (Figure 10). Combining all the settling velocity and discharge cases resulted a sediment transport lag factor that was linear with settling velocity, with a best fit slope of 34 $(mm/s)^{-1}$. The regression was influenced by the fast settling sediment classes (3 mm s^{-1} for Q_r = 5,000 $m^3\ s^{-1}$ and 0.2 mm s^{-1} for the range of Q_r cases) that are less well constrained,

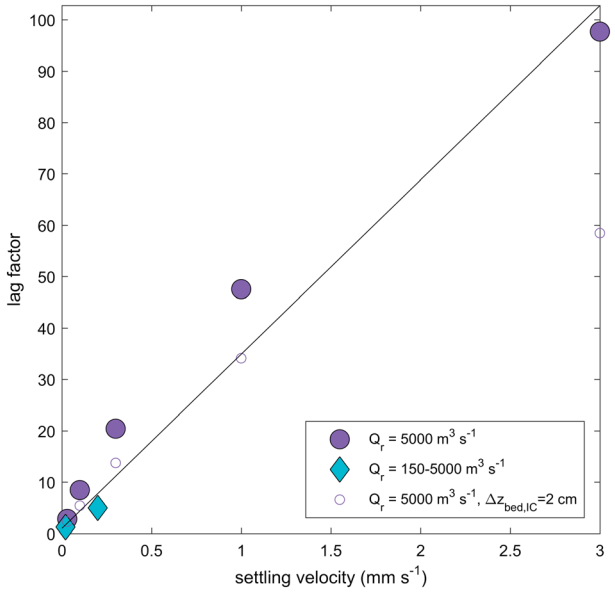

Figure 10. Suspended sediment lag factor versus setting velocity. The lag factors are from the slope of the age versus advective time scale in Figure 9 and represent factor by which sediment transport is slower than the water volume transport. The regression line is lag = 34 w_s + 1. The larger, colored markers have initial bed sediment thickness of 20 cm, while the smaller, dark gray circle circles represent an initial bed thickness of 2 cm.

so this may, in fact, underestimate the lag, and correspondingly sediment age. For example, excluding the w_s = 3 mm s^{-1} size class yields a best fit lag factor that is 47 times the settling velocity.

The initial thickness of the bed sediment in the model also plays a role in the transport rate, albeit much less than the variation with settling velocity. In most simulations, the initial bed thickness was 0.2 m to provide sufficient sediment supply, and deposition or erosion over the simulations amounted to a few centimeters or less. The bed was a single layer in the model, so any sediment that deposits instantly is mixed with sediment already on the bed, and subsequent resuspension is proportional to the amount of each sediment class in the bed. For the case with constant Q_r = 5,000 m^3 s^{-1}, reducing the initial bed thickness to 0.02 m did increase the calculated transport speeds. The lag factors between age and advection still scaled linearly with settling velocity but decreased slightly (Figure 10). For w_s < 3 mm s^{-1}, the best fit slope was a lag 34 times the settling velocity (in mm s^{-1}), compared with a slope of 47 with the initial bed thickness of 0.2 m. The appropriate thickness for bed sediment active at seasonal to interannual time scales is difficult to constrain, but recent observations from the Hudson and from the Penobscot estuary suggest active layer thicknesses of 5 cm to >10 cm (Geyer & Ralston, 2018; Woodruff et al., 2001). The uncertainty in the thickness in the active bed appears to affect the transport speeds by about 50%, while the settling velocity introduces orders of magnitude of variability. Similarly, the number of vertical layers prescribed in the bed model formulation would affect the vertical distribution of newly deposited sediment and thus could result in faster transport times for a given size class. This study did not examine in detail the role of the bed model, but it merits further investigation.

4.4. Sediment Age Distribution

The average sediment age for suspended sediment is well described by the advection time scale and settling velocity, but the bin averaging by distance along the river masks spatial heterogeneity associated with the bathymetry. In the deeper channel where velocity and stress were greater, suspended sediment age was less than in depositional, retentive areas on lateral shoals (Figure 11). Similarly, the age of sediment on the bed increased with distance along the river and had lateral structure corresponding with the bathymetry. As with suspended sediment, the age of sediment on the bed was greater in depositional regions than in the center of the channel.

At any location along the river, sediment on the bed was older than sediment in the water column (Figure 11). Suspended sediment in each size class advected seaward at the mean velocity times the lag factor for its settling velocity, and that scaling predominantly determined the age of suspended sediment at a location. Some of that suspended sediment deposited on the bed, and that newly deposited sediment mixed with older, previously deposited sediment. As a reminder, the age calculations only quantify new sediment input from the watershed, independent of the sediment on the bed at the start of the simulation. The age of sediment on the bed is the weighted average of the newly delivered sediment and sediment deposited earlier in the simulation, and the bed sediment continues to age in place with time. The youngest sediment on the bed at a location along the river took the advective time scale for suspended sediment (a_{ssc}, equation (1)) to travel from the head of tides to that point and then deposited. The oldest sediment was released at the start of the simulation, deposited at that location, and aged in the bed ever since. Assuming a relatively steady rate of deposition, a scaling for the age of sediment on the bed (a_{bed}) is the average of the advective time scale for that sediment class (youngest sediment) and the time since the start of the simulation (t_{sim}) (oldest sediment):

$$a_{bed} = \frac{1}{2}(\lambda_{ws} t_{adv} + t_{sim}) \quad (2)$$

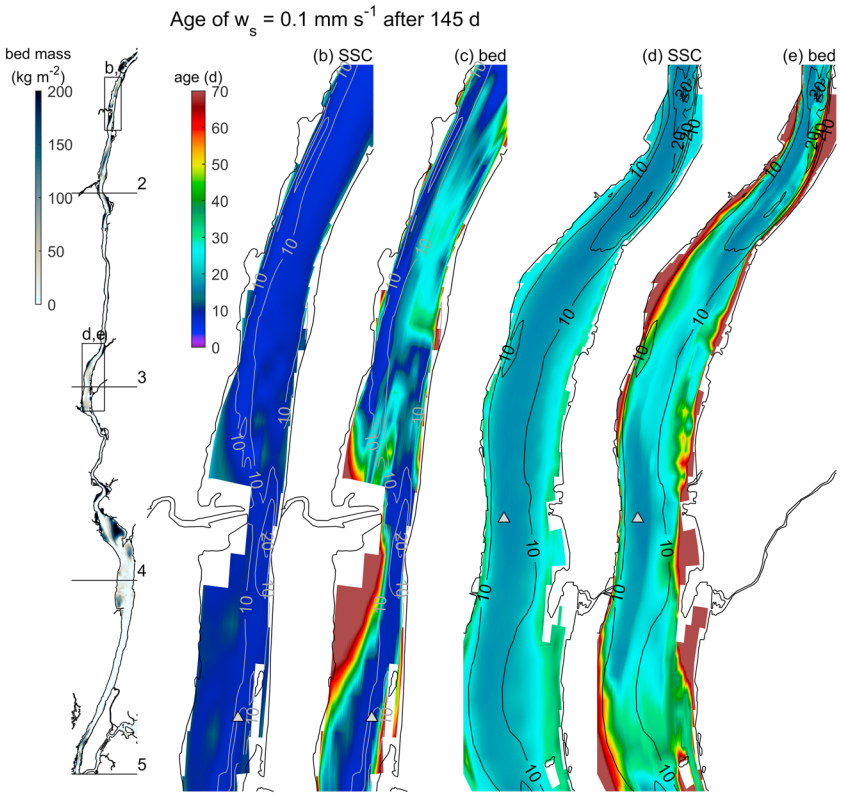

Figure 11. Maps of suspended and bed sediment age for settling velocity of 0.1 mm s^{-1}. The results are from the end of a simulation with constant discharge of 5,000 m^3 s^{-1} (145 day duration). (a) Mass distribution of sediment from river inputs. (b, c) Maps of suspended sediment age and bed sediment age near Tivoli (as in Figure 6a). (d, e) Maps of suspended sediment age and bed sediment age near Poughkeepsie and Newburgh (as in Figure 6b). Bathymetry contours are plotted along with locations of observations. Note the calculated age applies only to sediment introduced with the river discharge since the start of the simulation and does not include sediment starting on the bed that may in reality be much older.

Maps of bed sediment age (Figure 11) illustrate the spatial heterogeneity between the channel, where bed ages were similar to suspended sediment, and the more depositional shoals where the bed was much older than the suspended sediment. The scaling in equation (2) applies to the depositional regions that are continuously accumulating new sediment, so the average age of the bed increases with the length of the simulation. The example shown uses Q_r = 5,000 m^3 s^{-1} and for other discharge conditions the transition between erosional channel and depositional shoals might vary in detail, but conceptually, the strong lateral partitioning in sedimentary conditions is consistent with geophysical observations (Nitsche et al., 2007).

Based on the discharge and settling velocity, we can calculate the mean age of suspended sediment with distance along the river, recognizing that spatial variability is introduced by the realistic bathymetry. Because the sediment transport rates were much slower than the mean river velocity, even for the high discharge case (5,000 m^3 s^{-1}, u_r = 0.3–2 m s^{-1}) the sediment transport for settling velocities greater than ~0.5 mm s^1 took weeks to months to equilibrate with the input. High discharge periods typically last days (storm events) to weeks (spring freshet), and as river velocity decreases the time to reach equilibrium increases. For most of the sediment most of the time, the system is far from equilibrium, so a realistic evaluation of sediment age has to account for seasonal to interannual variability in river discharge as well as the differences in transport rate by sediment size class.

To extend the age results beyond the model simulation periods of several months, we used the historical discharge record to consider the statistics of transport time scales for water and sediment. The observed river discharge from the Mohawk and Upper Hudson dating back to 1917 is used to represent the temporal variability in forcing (Figure 12). To account for inputs from ungauged tributaries, the Mohawk and Upper Hudson discharge is multiplied by 1.4 (Wall et al., 2008). For any location along the river, the discharge time series and

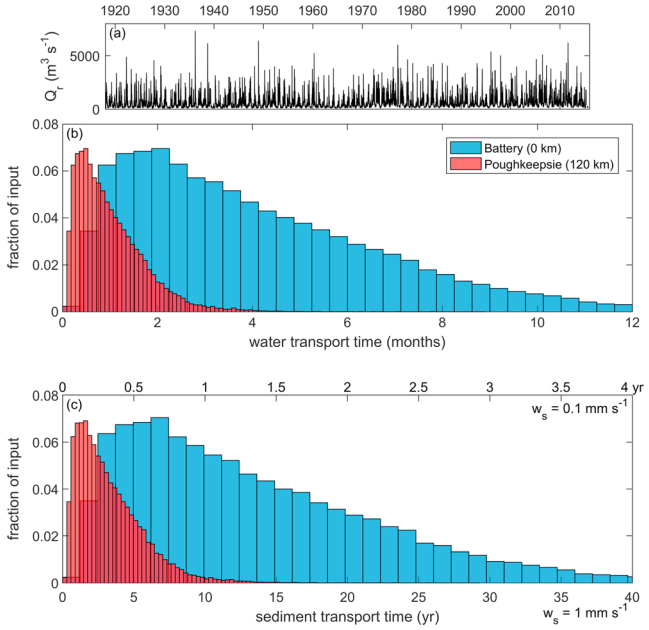

Figure 12. Age distributions based on advective time scales and historical discharge. (a) Discharge time series based on observations of the Mohawk (at Cohoes) and Upper Hudson (at Waterford) multiplied by 1.4 to represent tributary inputs to the Lower Hudson. (b) Distribution of transport time scales for water to travel from the head of tide (240 km) to Poughkeepsie (120 km) and the Battery (0 km). (c) Distribution of suspended sediment ages at the same locations based on the discharge time series and lag factors for settling velocities of 0.1 mm s^{-1} (top axis labels) and 1 mm s^{-1} (bottom axis labels). Note that water transport time is plotted in months and sediment ages in years.

average cross-sectional area landward of that point can be used to calculate a distribution of advective time scales for water (Figure 13b). Near Poughkeepsie (120 km), above which is almost always fresh, the mode of the advective time scale is about 0.5 months, with a skewed distribution toward a few months during low discharge. The travel time for water to the Battery (0 km) has similar shape but much longer time scale, with a mode of 2 months and a tail at more than 1 year.

The age distribution of sediment associated with a particular discharge event depends both on settling velocity and the time history of river discharge. The sediment input is highly nonlinear (Figure 3), but the model and observations indicate that transport in the tidal river scales linearly with discharge, so for a sufficiently long integrating time we can use the discharge time series to represent statistically the sediment travel time. The sediment transport time depends simply on the transport time for water (Figure 12b) and the lag factor for that settling velocity (Figure 10). For w_s = 1 mm s^{-1}, the lag factor of about 40 corresponds with sediment transport times from the tidal limit (240 km) to Poughkeepsie (120 km) of 1.5 years (mode) to 5–10 years or more in the tail of the distribution. The lag factor scales linearly with w_s, so transport times for 0.1 mm s^{-1} are a factor of 10 less, or a few months to a year. Transport times to the Battery are about 5 times that to Poughkeepsie. For w_s = 1 mm s^{-1}, the mode is about 7 years and the tail extends out several decades, while for w_s = 0.1 mm s^{-1} the transport time scales are 0.5 to 5 years. Note that the simple conceptual model was developed based on the sediment transport rates in the fresh tidal river and therefore likely represents a lower bound on transport time once sediment reaches the saline estuary. Geochemical and physical observations in the Lower Hudson estuary have found significant landward transport and recycling of sediment from New York Harbor (Feng et al., 1999; Geyer et al., 2001), as trapping by estuarine processes makes seaward transport less efficient and the estuary more retentive than the fresh tidal river. Additionally, flocculation in the estuary will shift some of the finer sediment into faster settling flocs, effectively increasing the transport time for some of the sediment that moved seaward through the tidal river more rapidly as individual particles.

4.5. Advection, Deposition, and Settling Velocity

In addition to a lag in the sediment transport compared with the river velocity, the model results show that the loss due to deposition, and thus the equilibrium transport rate depends on settling velocity (Figure 7). A simple conceptual model can be used to characterize the rate of sediment loss along the tidal river, where the decrease in transport is due to settling in depositional areas. For a segment of river with length Δx and discharge Q_r, the sediment mass balance can be written as

$$\frac{\Delta M}{\Delta t} = Q_r C_{\text{in}} - Q_r C_{\text{out}} - C w_s B_s \Delta x, \tag{3}$$

where $\Delta M/\Delta t$ is the rate of change of sediment mass in that segment, w_s is the settling velocity, B_s is the width of the channel that is depositional, and C_{in}, C_{out}, and C are concentrations upstream, downstream, and in the segment. The depositional width B_s is less than the total channel width (B) because it does not include the higher-energy flow regions that do not accumulate fine sediment (Figure 11). The discharge Q_r is uniform so spatial gradients in transport are due to a decrease in sediment concentration along the river due to settling, the third term on the right in (3). This is the same as an advection-reaction model with the time constant for the reaction rate $k = w_s/H_s$, where H_s is the water depth where settling occurs. In the limit of small Δx the solution to (3) can be written as

$$C(x) = C_0 \exp\left(-\delta \frac{w_s}{H_s} t_{\text{adv}} \frac{B_s}{B}\right), \tag{4}$$

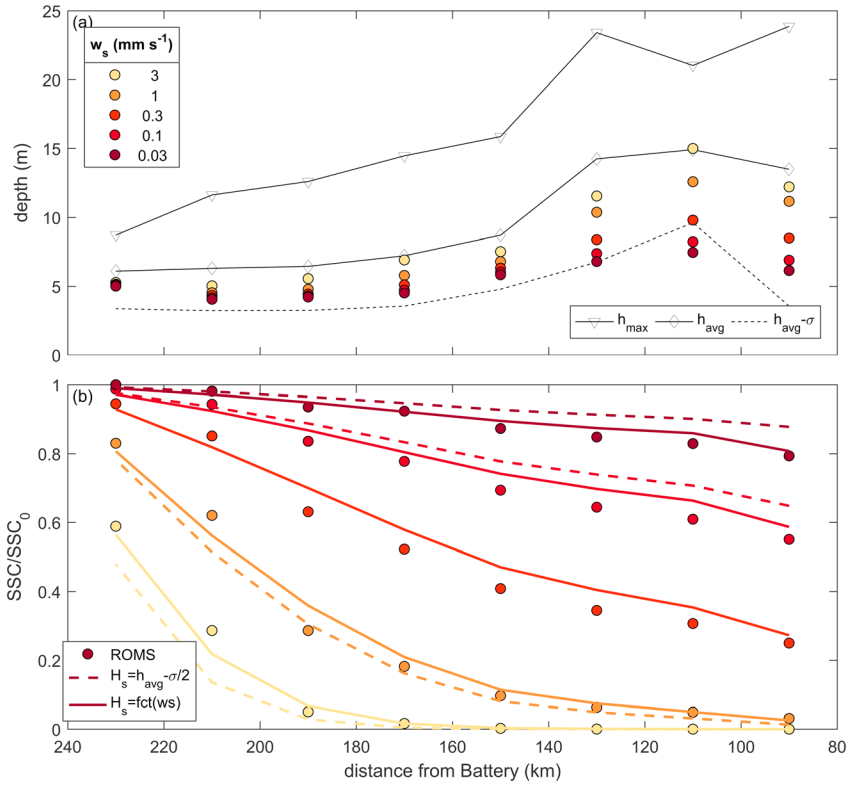

Figure 13. Modeling the decrease in sediment transport along the river by advection and settling. (a) In 30 km segments along the river, mass-weighted average of the water depth where sediment is deposited, for each of the settling velocity classes. Also shown is the mean thalweg depth (h_{max}), the mean depth (h_{avg}), and the mean depth − 1 standard deviation (σ) in the 30 km segments. (b) Average SSC with distance relative to the input at the head of tide (SSC_0). Also plotted are advection-reaction model (equation (4)) results with the settling depth $H_s = h_{avg} - 0.5*\sigma$ and with $H_s = h_{avg} - f*\sigma$, where f varies linearly between 0 and 1 for the settling velocity classes from 3 to 0.03 mm s^{-1}. For w_s = 0.3 mm s^{-1}, f = 0.5 and the two equations are the same.

where C_0 is the input concentration, $t_{adv}(x)$ is the advective time scale, which is nominally $x/(Q_r/A)$ with x the distance from the head of tide. We have included a duty cycle factor δ because settling occurs predominantly at slack tide, which represents only a small fraction of the tidal cycle.

The applicability of the conceptual model can be tested by plotting the sediment concentration along the river relative to the input concentration at the tidal limit (SSC_0) for the Q_r = 5,000 m^3 s^{-1} case (Figure 13). The advection-reaction model requires determining the average water depth for depositional regions, H_s. In the Hudson, both the mean and thalweg depth increase with distance downriver, with the thalweg about 1.5 to 2 times the mean. Deposition occurs preferentially in shallower regions on the edges of the channel (Figures 6 and 11), as shown in the mass-weighted average depth of where new sediment deposited for each size class (Figure 13a). The average depth of deposition was even shallower for the slower settling size classes. The longer that sediment remains in the water column each tide, the more it can disperse into lower energy regions and deposit. In contrast, faster settling size classes remained predominantly in the deeper channel regions. The threshold stress for resuspension was held constant for these cases to focus on settling, but in reality they covary and that could also affect the lateral distribution of resuspension.

First, we apply the advection-reaction model using a single settling depth for all size classes, setting H_s to be halfway between the average depth and the average depth minus 1 standard deviation: $H_s = h_{avg} - 0.5*\sigma$. The depositional width B_s is assumed to be half the total river width, and based on comparison with the ROMS results, the duty cycle δ is set to 1/5, which corresponds to ~70 min of settling time during slack tide. These parameters are for scaling purposes, but they are all consistent with physical expectations. Using the range of settling velocities and the advective time scale for water, we find that the simple advection-reaction model explains much of the variation in SSC along the river and among the size classes (Figure 13b).

Alternatively, we can account for the spatial difference in where sediment settles by size class, with finer particles depositing in shallower regions at the river edges (Figure 13a). For simplicity, we allow H_s to vary linearly among the sediment size classes, from $H_s = h_{avg}$ for $w_s = 3$ mm s^{-1} to $H_s = h_{avg} - \sigma$ for $w_s = 0.03$ mm s^{-1}. This empirical approach is consistent with our conceptual understanding, and the modified H_s accounts for much of the residual error compared with using a single H_s for all size classes (Figure 13b).

5. Discussion

5.1. Settling Velocity and Sediment Transport

The model results highlight the extreme sensitivity of the sediment transport rate and efficiency to settling velocity. Settling velocities of discrete particles corresponds with grain size, although flocculation can greatly increase the settling velocity of small particles, particularly in the saline estuary. In the tidal river at Poughkeepsie, the suspended sediment is predominantly fine ($<$63 μm) (Wall et al., 2008), but particle settling velocities range from 3 mm s^{-1} for coarse silt to less than 0.01 mm s^{-1} for clay. Suspended sediment observations at Poughkeepsie are consistent with the simultaneous presence of a washload and larger particles that are resuspended and deposited each tide (Wall et al., 2008). In the upper saline estuary (Haverstraw Bay), the primary particle size of suspended sediment had a bi-modal distribution, with peaks at $<$5 μm and 22–63 μm (Menon et al., 1998). Characterizing these ranges as "fine" and "coarse," that study found that the ratio of fine to coarse increased from about 1 near the head of tides to about 2 in the lower tidal river. The clay size range ($<$2 μm) was 11% of the particles in samples from the Mohawk and Upper Hudson but increased to 26% at Poughkeepsie, suggesting deposition of coarser silt along the tidal river. The increase in finer particles is consistent with a muddier bed toward the mouth (Nitsche et al., 2007), as coarser particles settle closer to the tributary inputs.

Direct measurements of settling velocity measurements remain a major observational challenge. A Rouse profile can be fit to suspended sediment to calculate an effective settling velocity (Sassi et al., 2013) including with multiple size classes (Fain et al., 2001), but the approach is difficult to constrain and spatial gradients complicate the analysis. Rouse profile estimates in the saline Hudson found settling velocities from 0.6 to 6 mm s^{-1} and a characteristic value of 2 mm s^{-1} (Orton & Kineke, 2001). Primary particle size distributions can characterize spatial and temporal trends in the sediment composition but the connection to settling velocity depends on the suspended material (e.g., mineral and organic composition) and flow conditions (turbulence and salinity). Given the sensitivity of the transport efficiency and sediment age to settling velocity, better characterization of the settling velocity distribution in the environment would be the most effective means of reducing uncertainty in sediment transport modeling.

5.2. Time Scales of Transport

High discharge periods that deliver sediment to the tidal river and also correspond with increased SSC in the saline estuary (Geyer et al., 2001). During the spring freshet, deposition increases in the lower estuary near the Battery, and in the following months as discharge decreases this sediment is eroded and sedimentation increases 20 km landward in the lower ETM (Woodruff et al., 2001). While it is tempting to assume, the increased SSC and deposition rates in the estuary are due to the increased sediment load from the watershed, the observational and model results here indicate otherwise. In addition to the increased supply, high discharge increases bed stress and mobilizes sediment in the tidal river and estuary, thereby increasing the total seaward sediment transport, although little of that sediment came from the discharge event. Seaward advection of the salinity intrusion also exposes regions of the estuary that were previously stratified to greater bed stresses and greater erosion rates of a tidal fresh regime (Ralston et al., 2013). Thus, much of the seasonal increase in SSC in the saline estuary is due to remobilization of bed sediment rather than new inputs from the watershed.

Rather than days to weeks of a high discharge event, the time scales for transport of sediment to the estuary are years to decades. Sediment age, or how long sediment is retained in the tidal river and estuary, has implications for the fate of organic constituents and metals that are preferentially associated with particles. For particulate organic matter, the amount of consumption and transformation in an estuary increases with the residence time (Middelburg & Herman, 2007). The results here suggest that the residence time of the tidal fresh region could affect the composition of terrestrial organic matter that reaches the saline estuary.

Observations over 3 years in the tidal fresh Hudson found that particulate organic carbon concentration depended more on processes in the tidal river than the external loading from tributaries, consistent with a long residence time and extensive internal processing (Findlay et al., 1991). Note that the sediment age calculated here represents time in the tidal river and estuary, rather than the much longer time scales for the age of organic carbon that also depend on characteristics of the aquatic, terrigenous, and anthropogenic carbon sources (Canuel & Hardison, 2016).

Time scales of recovery for estuaries with contaminated sediments also depend on transport time scales. As with many urbanized rivers, the Hudson has a history of industrialization and contaminant inputs, including polychlorinated biphenyls (PCBs) and heavy metals. A major PCB source was in the Upper Hudson, and PCBs are now distributed all along the tidal river and estuary. PCB concentration chronologies from cores give recovery time scales of several years to more than a decade (Bopp & Simpson, 1989; Rodenburg & Ralston, 2017). In the Columbia River, releases of radioactive contaminants from the Hanford Site upstream of the tidal limit were used as tracers to characterize sediment transport in the tidal river and estuary (Hubbell & Glenn, 1973). Distributions of particle-associated radionuclides had characteristics consistent with many of the results found here, including lateral partitioning between deeper, dynamic channel regions with coarser bed sediment and shoals with finer-grained sediment, high deposition rates (8.6 cm/yr), and higher radionuclide concentrations. The 1965 survey was about 20 years after the contaminant release began, and while about 66% of the radioactivity was found in the upper 20 cm of the bed, some locations had radioactivity up to 1.5 m below the bed surface (Hubbell & Glenn, 1973). Particle transport rates based on the decay of radioactivity downstream were found to decrease as the mean particle size increased, consistent with the inverse dependence on settling velocity found here.

6. Conclusions

The Hudson watershed, tidal river, and estuary have an extensive observational record with which we can characterize the magnitude and time scales of terrestrial material fluxes to the coastal ocean. Discrepancies between the sediment discharge from tributary rivers and seaward transport measured in the lower tidal river indicate significant deposition in the tidal river and delay in sediment discharge relative to inputs. The watershed loading is highly nonlinear, with a discharge dependence that is nearly cubic, but seaward transport in the tidal river is closer to linear with discharge (Figure 3). Consequently, sediment delivery during discharge events greatly exceeds the transport in the tidal river and much of that new sediment remains on the bed for months to years after events.

We used a model with realistic bathymetry but idealized forcing to characterize how transport in the tidal river depends on the forcing (river discharge) and sediment characteristics (settling velocity). To quantify time scales of transport, we adapted the tracer age model to sediment input from the watershed. Both observations and the model show that suspended sediment from discharge events advects seaward at a rate much slower than the mean river velocity. With the model, we find that the age of suspended sediment is well characterized by the advective time scale for water times a lag factor that scales linearly with settling velocity. The wide range of settling velocities of particles in the environment equates to a wide range of transport time scales. Applying the suspended sediment age scaling to the observed river discharge in the Hudson results in transport times through the tidal river and to the ocean of years for fine silt (w_s = 0.1 mm s^{-1}) to decades for coarse silt (w_s = 1 mm s^{-1}) (Figure 12).

In addition to the timing of sediment delivery to the ocean, settling velocity affects the fraction of sediment that is retained in the tidal river. Transport efficiency decreases with settling velocity, and a simple advection-reaction equation can represent the decrease in SSC and sediment transport due to settling with distance along the river. Deposition occurs primarily on lower energy shoals and sediment inside embayments, while the channel bed is coarser and more dynamic. The lateral partitioning of trapping and the sorting of particles along the tidal river by preferential loss of faster settling sediment is consistent with the observed bed composition (Nitsche et al., 2007).

Acknowledgments
This work was supported by Hudson River Foundation grant 004/13A and National Science Foundation grant 1325136. The authors thank three anonymous reviewers and the Associate Editor for constructive comments that improved the manuscript. Much of the observational data used in this study are available from public sources (USGS, NOAA, and HRECOS), and access to additional observational data and model results is available by contacting David Ralston (dralston@whoi.edu).

References

Abood, K. A. (1974). Circulation in the Hudson estuary. *Annals of the New York Academy of Sciences*, *250*(1), 39–111. https://doi.org/10.1111/j.1749-6632.1974.tb43895.x

Benoit, G., Wang, E. X., Nieder, W. C., Levandowsky, M., & Breslin, V. T. (1999). Sources and history of heavy metal contamination and sediment deposition in Tivoli South Bay, Hudson River, New York. *Estuaries*, *22*(2), 167–178. https://doi.org/10.2307/1352974

Bokuniewicz, H. J., & Ellsworth, J. M. (1986). Sediment budget for the Hudson system. *Northeastern Geology*, *8*(3), 156–164.

Bopp, R. F., & Simpson, H. J. (1989). Contamination of the Hudson River: The sediment record. *Contaminated Marine Sediments Assessment and Remediation*, 401–416.

Bowen, M. M. & Geyer, W. R. (2003). Salt transport and the time-dependent salt balance of a partially stratified estuary. *Journal of Geophysical Research*, *108*(C5), 3158. https://doi.org/10.1029/2001JC001231

Canuel, E. A., & Hardison, A. K. (2016). Sources, ages, and alteration of organic matter in estuaries. *Annual Review of Marine Science*, *8*(1), 409–434. https://doi.org/10.1146/annurev-marine-122414-034058

Chillrud, S. N., Bopp, R. F., Ross, J. M., Chaky, D. A., Hemming, S., Shuster, E. L., … Estabrooks, F. (2004). Radiogenic lead isotopes and time stratigraphy in the Hudson River, New York. *Water, Air, & Soil Pollution: Focus*, *4*(2/3), 469–482. https://doi.org/10.1023/B:WAFO.0000028372.87703.b7

Cook, T. L., Sommerfield, C. K., & Wong, K.-C. (2007). Observations of tidal and springtime sediment transport in the upper Delaware estuary. *Estuarine, Coastal and Shelf Science*, *72*(1-2), 235–246. https://doi.org/10.1016/j.ecss.2006.10.014

Deleersnijder, E., Campin, J.-M., & Delhez, E. J. M. (2001). The concept of age in marine modelling: I. Theory and preliminary model results. *Journal of Marine Systems*, *28*(3–4), 229–267. https://doi.org/10.1016/S0924-7963(01)00026-4

Delhez, E. J. M., Campin, J.-M., Hirst, A. C., & Deleersnijder, E. (1999). Toward a general theory of the age in ocean modelling. *Ocean Modelling*, *1*(1), 17–27. https://doi.org/10.1016/S1463-5003(99)00003-7

Delhez, E. J. M., & Wolk, F. (2013). Diagnosis of the transport of adsorbed material in the Scheldt estuary: A proof of concept. *Journal of Marine Systems*, *128*, 17–26. https://doi.org/10.1016/j.jmarsys.2012.01.007

Downing, J. (2006). Twenty-five years with OBS sensors: The good, the bad, and the ugly. *Continental Shelf Research*, *26*(17–18), 2,299–2,318. https://doi.org/10.1016/j.csr.2006.07.018

Downing-Kunz, M. A., & Schoellhamer, D. H. (2015). Suspended-sediment trapping in the tidal reach of an estuarine tributary channel. *Estuaries and Coasts*, *38*(6), 2198–2212. https://doi.org/10.1007/s12237-015-9944-4

Dunne, T., Mertes, L. A. K., Meade, R. H., Richey, J. E., & Forsberg, B. R. (1998). Exchanges of sediment between the flood plain and channel of the Amazon River in Brazil. *Geological Society of America Bulletin*, *110*(4), 450–467. https://doi.org/10.1130/0016-7606(1998)110%3C0450:EOSBTF%3E2.3.CO;2

Ensign, S. H., Noe, G. B., & Hupp, C. R. (2014). Linking channel hydrology with riparian wetland accretion in tidal rivers. *Journal of Geophysical Research: Earth Surface*, *119*(1), 28–44. https://doi.org/10.1002/2013JF002737

Fain, A. M. V., Jay, D. A., Wilson, D. J., Orton, P. M., & Baptista, A. M. (2001). Seasonal and tidal monthly patterns of particulate matter dynamics in the Columbia River estuary. *Estuaries*, *24*(5), 770–786. https://doi.org/10.2307/1352884

Feng, H., Cochran, J. K., & Hirschberg, D. J. (1999). ^{234}Th and ^{7}Be as tracers for the transport and dynamics of suspended particles in a partially mixed estuary. *Geochimica et Cosmochimica Acta*, *63*(17), 2487–2505. https://doi.org/10.1016/S0016-7037(99)00060-5

Feng, H., Cochran, J. K., Hirschberg, D. J., & Wilson, R. E. (1998). Small-scale spatial variations of natural radionuclide and trace metal distributions in sediments from the Hudson River estuary. *Estuaries*, *21*(2), 263–280. https://doi.org/10.2307/1352474

Findlay, S., Pace, M., & Lints, D. (1991). Variability and transport of suspended sediment, particulate and dissolved organic carbon in the tidal freshwater Hudson River. *Biogeochemistry*, *12*(3), 149–169. https://doi.org/10.1007/BF00002605

Fricke, A. T., Nittrouer, C. A., Ogston, A. S., Nowacki, D. J., Asp, N. E., Filho, S., … Jalowska, A. M. (2017). River tributaries as sediment sinks: Processes operating where the Tapajós and Xingu Rivers meet the Amazon tidal river. *Sedimentology*, *64*(6), 1731–1753. https://doi.org/10.1111/sed.12372

Geyer, W. R., & Ralston, D. K. (2018). A mobile pool of contaminated sediment in the Penobscot estuary, Maine, USA. *Science of the Total Environment*, *612*, 694–707. https://doi.org/10.1016/j.scitotenv.2017.07.195

Geyer, W. R., Woodruff, J. D., & Traykovski, P. (2001). Sediment transport and trapping in the Hudson River estuary. *Estuaries*, *24*(5), 670–679. https://doi.org/10.2307/1352875

Glysson, G. D. (1987). Sediment-transport curves. US Geological Survey.

Godin, G. (1999). The propagation of tides up rivers with special considerations on the Upper Saint Lawrence River. *Estuarine, Coastal and Shelf Science*, *48*(3), 307–324. https://doi.org/10.1006/ecss.1998.0422

Gong, W., & Shen, J. (2010). A model diagnostic study of age of river-borne sediment transport in the tidal York River estuary. *Environmental Fluid Mechanics*, *10*(1-2), 177–196. https://doi.org/10.1007/s10652-009-9144-5

Goodbred, S. L. Jr., & Kuehl, S. A. (1998). Floodplain processes in the Bengal Basin and the storage of Ganges–Brahmaputra river sediment: An accretion study using ^{137}Cs and ^{210}Pb geochronology. *Sedimentary Geology*, *121*(3-4), 239–258. https://doi.org/10.1016/S0037-0738(98)00082-7

Gray, J. R., & Simões, F. J. (2008). Estimating sediment discharge. In *Sedimentation engineering: Processes, measurements, modeling, and practice*, (pp. 1067–1088). https://doi.org/10.1061/9780784408148.apd

Haidvogel, D. B., Arango, H., Budgell, W. P., Cornuelle, B. D., Curchitser, E., Di Lorenzo, E., … Wilkin, J. (2008). Ocean forecasting in terrain-following coordinates: Formulation and skill assessment of the Regional Ocean modeling system. *Journal of Computational Physics*, *227*(7), 3595–3624. https://doi.org/10.1016/j.jcp.2007.06.016

Hoitink, A. J. F., & Jay, D. A. (2016). Tidal river dynamics: Implications for deltas. *Reviews of Geophysics*, *54*(1), 240–272. https://doi.org/10.1002/2015RG000507

Hubbell, D. W. & Glenn, J. L. (1973). Distribution of radionuclides in bottom sediments of the Columbia River estuary (USGS Numbered Series No. 433L) (p. 62). U.S. Geological Survey. Retrieved from https://pubs.er.usgs.gov/publication/pp433L

Klingbeil, A. D., & Sommerfield, C. K. (2005). Latest Holocene evolution and human disturbance of a channel segment in the Hudson River estuary. *Marine Geology*, *218*(1–4), 135–153. https://doi.org/10.1016/j.margeo.2005.02.026

McHugh, C. M. G., Pekar, S. F., Christie-Blick, N., Ryan, W. B. F., Carbotte, S., & Bell, R. (2004). Spatial variations in a condensed interval between estuarine and open-marine settings: Holocene Hudson River estuary and adjacent continental shelf. *Geology*, *32*(2), 169–172. https://doi.org/10.1130/G20150.1

Meade, R. H. (1996). River-sediment inputs to major deltas. In *Sea-level rise and coastal subsidence* (pp. 63–85). Dordrecht, Netherlands: Springer. https://doi.org/10.1007/978-94-015-8719-8_4

Menon, M. G., Gibbs, R. J., & Phillips, A. (1998). Accumulation of muds and metals in the Hudson River estuary turbidity maximum. *Environmental Geology*, *34*(2–3), 214–222. https://doi.org/10.1007/s002540050273

Mercier, C., & Delhez, E. J. M. (2007). Diagnosis of the sediment transport in the Belgian coastal zone. *Estuarine, Coastal and Shelf Science*, *74*(4), 670–683. https://doi.org/10.1016/j.ecss.2007.05.010

Middelburg, J. J., & Herman, P. M. J. (2007). Organic matter processing in tidal estuaries. *Marine Chemistry*, *106*(1–2), 127–147. https://doi.org/10.1016/j.marchem.2006.02.007

Milliman, J. D., & Farnsworth, K. L. (2013). *River discharge to the coastal ocean: A global synthesis*. Cambridge: Cambridge University Press.

Milliman, J. D., Huang-ting, S., Zuo-sheng, Y., Mead, H., & R. (1985). Transport and deposition of river sediment in the Changjiang estuary and adjacent continental shelf. *Continental Shelf Research*, *4*(1–2), 37–45. https://doi.org/10.1016/0278-4343(85)90020-2

Mukai, A. Y., Westerink, J. J., Luettich Jr, R. A., & Mark, D. (2002). Eastcoast 2001: A tidal constituent database for western North Atlantic, Gulf of Mexico, and Caribbean Sea. DTIC Document.

Nash, D. B. (1994). Effective sediment-transporting discharge from magnitude-frequency analysis. *Journal of Geology*, *102*(1), 79–95. https://doi.org/10.1086/629649

Nitsche, F. O., Kenna, T. C., & Haberman, M. (2010). Quantifying 20th century deposition in complex estuarine environment: An example from the Hudson River. *Estuarine, Coastal and Shelf Science*, *89*(2), 163–174. https://doi.org/10.1016/j.ecss.2010.06.011

Nitsche, F. O., Ryan, W. B. F., Carbotte, S. M., Bell, R. E., Slagle, A., Bertinado, C., … McHugh, C. (2007). Regional patterns and local variations of sediment distribution in the Hudson River estuary. *Estuarine, Coastal and Shelf Science*, *71*(1-2), 259–277. https://doi.org/10.1016/j.ecss.2006.07.021

Nittrouer, C. A., Kuehl, S. A., Sternberg, R. W., Figueiredo, A. G. Jr., & Faria, L. E. C. (1995). An introduction to the geological significance of sediment transport and accumulation on the Amazon continental shelf. *Marine Geology*, *125*(3–4), 177–192. https://doi.org/10.1016/0025-3227(95)00075-A

Nowacki, D. J., Ogston, A. S., Nittrouer, C. A., Fricke, A. T., & Van, P. D. T. (2015). Sediment dynamics in the lower Mekong River: Transition from tidal river to estuary. *Journal of Geophysical Research: Oceans*, *120*(9), 6363–6383. https://doi.org/10.1002/2015JC010754

Orton, P. M., & Kineke, G. C. (2001). Comparing calculated and observed vertical suspended-sediment distributions from a Hudson River estuary turbidity maximum. *Estuarine, Coastal and Shelf Science*, *52*(3), 401–410. https://doi.org/10.1006/ecss.2000.0747

Panuzio, F. L. (1965). Lower Hudson River siltation. In *Proceedings of the 2nd Federal Interagency Sedimentation Conference* (pp. 512–550). Jackson, MS: Agricultural Research Service.

Ralston, D. K., & Geyer, W. R. (2009). Episodic and long-term sediment transport capacity in the Hudson River estuary. *Estuaries and Coasts*, *32*(6), 1130–1151. https://doi.org/10.1007/s12237-009-9206-4

Ralston, D. K., Geyer, W. R., & Lerczak, J. A. (2008). Subtidal salinity and velocity in the Hudson River estuary: Observations and modeling. *Journal of Physical Oceanography*, *38*(4), 753–770. https://doi.org/10.1175/2007JPO3808.1

Ralston, D. K., Geyer, W. R., & Warner, J. C. (2012). Bathymetric controls on sediment transport in the Hudson River estuary: Lateral asymmetry and frontal trapping. *Journal of Geophysical Research*, *117*, C10013. https://doi.org/10.1029/2012JC008124

Ralston, D. K., Warner, J. C., Geyer, W. R., & Wall, G. R. (2013). Sediment transport due to extreme events: The Hudson River estuary after tropical storms Irene and lee. *Geophysical Research Letters*, *40*(20), 5451–5455. https://doi.org/10.1002/2013GL057906

Rodenburg, L. A., & Ralston, D. K. (2017). Historical sources of polychlorinated biphenyls to the sediment of the New York/New Jersey Harbor. *Chemosphere*, *169*, 450–459. https://doi.org/10.1016/j.chemosphere.2016.11.096

Sanford, L., Suttles, S., & Halka, J. (2001). Reconsidering the physics of the Chesapeake Bay estuarine turbidity maximum. *Estuaries and Coasts*, *24*(5), 655–669. https://doi.org/10.1007/BF02804824

Sassi, M. G., Hoitink, A. J. F., Vermeulen, B., & Hidayat, H. (2013). Sediment discharge division at two tidally influenced river bifurcations. *Water Resources Research*, *49*(4), 2119–2134. https://doi.org/10.1002/wrcr.20216

Schubel, J. R., & Hirschberg, D. J. (1978). Estuarine graveyards, climatic change, and the importance of the estuarine environment. In *Estuarine interactions* (pp. 285–303). New York: Academic Press. https://doi.org/10.1016/B978-0-12-751850-3.50024-8

Shchepetkin, A. F., & McWilliams, J. C. (2005). The Regional Oceanic Modeling System (ROMS): A split-explicit, free-surface, topography-following-coordinate oceanic model. *Ocean Modelling*, *9*(4), 347–404. https://doi.org/10.1016/j.ocemod.2004.08.002

Sommerfield, C. K. (2006). On sediment accumulation rates and stratigraphic completeness: Lessons from Holocene ocean margins. *Continental Shelf Research*, *26*(17–18), 2225–2240. https://doi.org/10.1016/j.csr.2006.07.015

Sommerfield, C. K., & Wong, K.-C. (2011). Mechanisms of sediment flux and turbidity maintenance in the Delaware estuary. *Journal of Geophysical Research*, *116*, C01005. https://doi.org/10.1029/2010JC006462(C1).

Swaney, D. P., Sherman, D., & Howarth, R. W. (1996). Modeling water, sediment and organic carbon discharges in the Hudson-Mohawk Basin: Coupling to terrestrial sources. *Estuaries*, *19*(4), 833–847. https://doi.org/10.2307/1352301

Syvitski, J. P. M. (2003). Supply and flux of sediment along hydrological pathways: Research for the 21st century. *Global and Planetary Change*, *39*(1-2), 1–11. https://doi.org/10.1016/S0921-8181(03)00008-0

Syvitski, J. P. M., Peckham, S. D., Hilberman, R., & Mulder, T. (2003). Predicting the terrestrial flux of sediment to the global ocean: A planetary perspective. *Sedimentary Geology*, *162*(1-2), 5–24. https://doi.org/10.1016/S0037-0738(03)00232-X

Traykovski, P., Geyer, R., & Sommerfield, C. (2004). Rapid sediment deposition and fine-scale strata formation in the Hudson estuary. *Journal of Geophysical Research*, *109*, F02004. https://doi.org/10.1029/2003JF000096

Wall, G., Nystrom, E., & Litten, S. (2008). Suspended sediment transport in the freshwater reach of the Hudson River estuary in eastern New York. *Estuaries and Coasts*, *31*(3), 542–553. https://doi.org/10.1007/s12237-008-9050-y

Warner, J. C., Geyer, W. R., & Lerczak, J. A. (2005). Numerical modeling of an estuary: A comprehensive skill assessment. *Journal of Geophysical Research*, *110*, C05001. https://doi.org/10.1029/2004JC002691

Warner, J. C., Rockwell Geyer, W., & Arango, H. G. (2010). Using a composite grid approach in a complex coastal domain to estimate estuarine residence time. *Computers & Geosciences*, *36*(7), 921–935. https://doi.org/10.1016/j.cageo.2009.11.008

Warner, J. C., Sherwood, C. R., Signell, R. P., Harris, C. K., & Arango, H. G. (2008). Development of a three-dimensional, regional, coupled wave, current, and sediment-transport model. *Computers & Geosciences*, *34*(10), 1284–1306. https://doi.org/10.1016/j.cageo.2008.02.012

Woodruff, J. D. (1999). Sediment deposition in the Lower Hudson River estuary (M.S. thesis). Massachusetts Institute of Technology/Woods Hole Oceanographic Institution.

Woodruff, J. D., Geyer, W. R., Sommerfield, C. K., & Driscoll, N. W. (2001). Seasonal variation of sediment deposition in the Hudson River estuary. *Marine Geology*, *179*(1–2), 105–119. https://doi.org/10.1016/S0025-3227(01)00182-7

Woodruff, J. D., Martini, A. P., Elzidani, E. Z., Naughton, T. J., Kekacs, D. J., & MacDonald, D. G. (2013). Off-river waterbodies on tidal rivers: Human impact on rates of infilling and the accumulation of pollutants. *Geomorphology*, *184*, 38–50. https://doi.org/10.1016/j.geomorph.2012.11.012

Zhang, W. G., Wilkin, J. L., & Schofield, O. M. E. (2009). Simulation of water age and residence time in New York Bight. *Journal of Physical Oceanography*, *40*(5), 965–982. https://doi.org/10.1175/2009JPO4249.1